Performance Benchmark of Planar Solid Oxide Cells Based on Material Development and Design.

David Udomsilp, Christian Lenser, Olivier Guillon, Norbert H. Menzler**

Dr. D. Udomsilp, Dr. C. Lenser, Prof. O. Guillon, Prof. N.H. Menzler
Forschungszentrum Jülich GmbH, Institute of Energy and Climate Research, Materials Synthesis and Processing (IEK-1), 52425 Jülich, Germany
E-Mail: d.udomsilp@fz-juelich.de , n.h.menzler@fz-juelich.de

Prof. O. Guillon
Jülich Aachen Research Alliance: JARA-ENERGY, 52425 Jülich, Germany

Keywords: SOFC, SOEC, PCFC

Abstract

Solid oxide cell technology currently attracts great attention due to its unique potential for substantially contributing to a carbon-neutral power supply. The variety in possible designs and applications – covering oxygen ion and proton conductors and the ability to convert surplus electricity to easily storable synthetic fuels as well as to produce electricity from these fuels according to demand and availability – provides the excellent position of solid oxide cells with regard to decentralized power generation and distribution. This paper serves as a reference work on cell performance, by highlighting specific advantages of the different cell types, designs, and materials with regard to certain operating conditions including challenges concerning operational modes, processing, and degradation. In conjunction with a critical examination in terms of relevance and technical feasibility, the data provided enable assessment of the general potential of the cell types for technology development and connect scientific research to industrial considerations.

1. Introduction

In order to limit human-made global warming, significant efforts worldwide are dedicated to carbon-neutral power generation and supply as an alternative to fossil-derived energy. Therefore,

great interest arises with regard to solid oxide cell (SOC) applications electrochemically converting the chemical energy of liquid or gaseous fuels into electricity and vice versa. The potential of the SOC technology to be a key aspect on the way to carbon-neutrality can be illustrated by the possible impact on the main sectors contributing to global CO_2 emissions. In 2016, only four sectors accounted for 93 % of global CO_2 emissions. The largest emitting sector was electricity and heat accounting for 42 % of emissions, followed by transport (24 %), industry (19 %) and buildings (8 %).[1] In all of these sectors, SOC-based systems offer the potential to reduce emissions, both through enhanced efficiency and the ability to utilize green fuels. SOC systems are particularly well-suited for flexible and decentralized power generation and distribution. In peak periods of renewable power generation from solar or wind, surplus electricity can be converted to synthetic fuels. These fuels can be efficiently stored and easily transported and reconverted to electricity and heat during peak load times or periods of limited availability of renewable energy sources. In industrial production of e.g. steel or glass, carbon emissions can be significantly reduced by use of H_2 generated from solid oxide electrolysis instead of using fossil sources for iron reduction or thermal management. In the transport sector, SOC-based range extenders for battery electric vehicles offer increased driving range, fast refueling, and fuel flexibility.[2-4] Moreover, the direct conversion enables superior efficiency compared to combustion-based technologies – especially under partial load – combined with silent operation and low or even zero emissions, depending on the fuel used. In this context, the term solid oxide cells describes oxygen ion (O^{2-}) conducting cells as well as proton (H^+) conducting cells made from oxide ceramics. Furthermore, it also includes the operation in fuel cell mode (generating electricity) or in electrolysis mode (converting electricity into chemicals). The denotation therefore covers four terms: solid oxide fuel cells and electrolysis cells (SOFC/SOEC) and proton conducting fuel cells and electrolysis cells (PCFC/PCEC).

Various SOC concepts were developed and several of them are commercially available or close to market entry.[5-12] The concepts differ in the species acting as charge carrier through the electrolyte, geometrical cell design, and mechanically supporting structure. First substantial progress was achieved by Westinghouse on tubular cells.[13-15] Advantageous properties of the tubular design are a well-supporting structure and a sealing area outside of the heated zone. Nowadays, the majority of concepts utilizes the planar cell design, as volumetric as well as gravimetric power density are typically higher and automation of the processing is easier enabling cheaper fabrication.[15-17]

Recently, significant progress in terms of volumetric power density was reported on microtubular cells.[18] However, even if these results are impressive and show potential for small-sized devices, scale-up is expected to prove challenging, as current collection and interconnection of tubular cells is substantially more complex compared to planar cells. The geometrical cell design, together with the materials of the cell components, roughly predefines parameters for cell operation. A typical line of development comprises the development of an operational cell, followed by enhancement of the cell performance, and subsequent optimization of the durability for long-term operation. General tendencies during the past decades point to lower operating temperature, higher performance, and most recently intensified focus on operation in electrolysis mode. The gathered experience and knowledge of electrochemical processes and degradation phenomena indicate that a single line of development is not expedient for universally meeting the current demands, but that cells must be specifically designed with regard to the intended application. That is the intended temperature of operation, stationary vs. mobile application, required power density (or acceptable size and weight of a system), etc.

Evaluation of the performance is a central step to match the goals set and the results achieved. This applies to a single-cell as well as to stacks and systems. Even when limiting the comparison of performance to single-cell measurements, there are various factors that need to be considered in order to assure the significance of the conclusions drawn. These include

- gas mixtures
- feed rates
- temperature
- cell dimensions and active area

In addition to a higher susceptibility to errors when using cells with small active area, the performance of very small button-cells often is difficult to directly transfer to full-size cells or even to stacks. With regard to practical applicability, manufacturing procedures need to be suitable for scale-up. In the case of stack testing, however, there are many additional influences complicating comparison of cell performance. Different stack designs and materials, less defined gas supply, quality of contacting, and temperature gradients have a pronounced impact on the power output. As an example, geometry and orientation of the air and fuel flow fields considerably influence

thermal management of a stack.[19-20] Co-flow, counter-flow or cross-flow exhibit different properties and can be advantageous according to certain operational modes and fuels (H_2, CH_4, etc.). Similarly, characteristic challenges are connected to system design, setup, and operation. Therefore, the topics of stack development and system integration are beyond the scope of this work since they provide data for separate extensive elaboration.

There are various excellent reviews and books available in the literature covering certain cell types, cell components, materials, manufacturing or mode of operation.[16-17, 21-41] These articles provide detailed insights into reaction mechanisms, nano-scale material properties, degradation phenomena, and economics of operation to name just a few. The aim of this paper is to present an overview of investigated material combinations and the obtained range of performance of planar SOCs, facilitating the assessment of the general potential of the cell types also for non-experts. This is based on concise description of the most important material properties and consideration of the influence of fabrication methods and test conditions. The technical feasibility of individual approaches and the state of development are taken into account, in order to emphasize especially promising approaches for systematic, application-oriented and -adapted development. With that, this comprehensive review connects scientific research of materials and design on single-cell level to industrial considerations for future technology development.

2. SOC processing, testing, setups, and materials

This section will be subdivided into four parts. The first subsection provides a brief introduction to processing methods and their influence on the cell properties, followed by a paragraph on the influence of testing conditions. The subsequent parts are dedicated to the type of material used as the electrolyte, oxygen ion conductors and proton conductors. The state-of-the-art materials are presented including the materials used for air and fuel electrodes. Additionally, examples of advanced processing and alternative materials, their performance and potential are discussed.

2.1. Processing of planar SOCs

Various methods with different sequences of fabrication of the single components are commonly used for manufacturing of planar SOCs. These include (sequential) tape casting, extrusion,

pressing, (thermal) spraying, screen printing, electrophoretic deposition (EPD) or thin-film techniques like sol-gel-based dip and spin coating, physical vapor deposition (PVD), and pulsed laser deposition (PLD).[17] Some advanced processing techniques aim at optimization of certain properties in a defined regime of operating conditions. **Table 1** summarizes processing methods along with information on the effort (such as time, cost, efficiency, scalability) associated with their use and properties of the fabricated layers. All of the presented technologies have been proven to be suitable to manufacture at least one of the layers of SOCs. However, in the view of industrialization (sequential) tape casting and screen printing have been established as the state-of-the-art processing methods.[42-45] This is due to their flexibility with regard to materials and layer thickness as well as their scalability, aiding mass production at low cost. In contrast, extrusion and pressing are mainly suitable for fabrication of rather thick substrates. Pressing is frequently used in lab-scale experiments as it is generally available and easily applicable, but does not allow for a continuous fabrication. Spraying methods suffer from moderate efficiency and difficult microstructure adjustment. For example, the fabrication of gas-tight electrolyte layers by atmospheric plasma spraying (APS) poses a challenge, same as providing sufficient open porosity of electrodes.[46] More sophisticated thermal spray processes such as high-velocity oxy-fuel spraying (HVOF) come with substantially higher cost of manufacturing. Thin-film techniques like chemical vapor deposition (CVD), PVD, PLD, and sol-gel-based methods typically provide high-quality layers but exhibit higher cost of fabrication because of increased invest or time consumption. For example, the vapor deposition techniques and PLD are performed in a vacuum chamber and sol-gel methods usually require multiple coating and thermal treatment steps. Therefore, the application of these methods is a tradeoff between acceptable cost and achievable benefit in performance. Especially for the deposition of electrolyte layers, the interplay between the surface to be coated and quality of the thin-film electrolyte is crucial. Very smooth and homogeneous surfaces are required in order to reliably deposit gas-tight layers.[47-48] Highly active electrode microstructures can be achieved by infiltration of nanoparticles/precursors [26, 49] in porous scaffolds previously fabricated by e.g. tape casting or by advanced processing methods like electrostatic spray deposition (ESD).[50-51] In case of infiltration-based techniques, long-term stability is an issue, as coarsening of the nanoparticles at elevated temperature causes performance degradation due to loss of active surface area. [26] Yet, infiltration may enable microstructural design beyond traditional sintering-based methods, given a thorough consideration of

microstructure evolution during operation. ESD provides increased flexibility with regard to the resulting microstructure [50] enabling tailored layer properties. As an example, a relatively dense interlayer between the electrolyte and the highly porous active electrode can improve adherence as well as interfacial resistance.[52] Again the influence of high-temperature exposure needs to be evaluated carefully as coarsening may degrade the electrode performance. For more detailed information on processing methods, the reader is referred to the relevant literature.[17, 23, 41, 53-55] What should be emphasized here is that processing predetermines the cell properties. The method itself, in combination with raw materials, their preconditioning, ink/suspension formulation, processing parameters, and subsequent steps like thermal treatments critically affects the microstructure of the functional layers and thus cell performance and durability. Hence, substantial improvements may be achieved solely by optimization of the fabrication in early stages of development.

Table 1: Processing methods for fabrication of planar SOC. SOA – state-of-the-art processing method used in industrial scale or well-established in lab-scale; "✓" –suitable for fabricating respective layer; "X" – not suitable.

Method	Effort & Properties	Thickness (dry layer)	Substrate	Fuel electrode	Electrolyte	Barrier (air side)	Air Electrode
Tape casting (single layer)	Scalable Continuous Industrialized	40-800 µm	SOA	SOA	SOA	✓	✓
Sequential tape casting	Same as above Single-step thermal treatment	5-800 µm (single layer) 250-800 µm (multi-layer)	SOA	SOA	SOA	✓ (limited)	✓ (impractical)
Tape casting/ lamination/ pressing	Limited scalability Single-step thermal treatment	40-800 µm (single layer) 250-1500 µm (multi-layer)	SOA	SOA	SOA	✓ (limited)	✓
Pressing	Lab-scale method Easy Low cost No thin films	> 1 mm	✓	✓ (limited)	✓ (limited)	✓ (limited)	✓ (limited)
Extrusion	Industrialized High wear Anisotropic aspect ratio and microstructure	> 500 µm	✓	✓ (limited)	X	X	X
Thermal spraying	Industrialized High invest	20-200 µm	X	✓	✓	✓	✓

	Moderate efficiency Microstructure control challenging						
Wet powder spraying	Industrialized Moderate efficiency Microstructure control challenging	20-200 µm	X	✓	✓	✓	✓
Screen printing	Industrialized Scalable Continuous (possible)	3-150 µm	X	SOA	SOA	SOA	SOA
EPD	Well-known in automotive corrosion protection (but not for ceramics) Careful suspension control required	< 5 µm (single layer)	X	✓	SOA	✓	✓
Sol-gel	Time-consuming Batch processing High quality possible	≈ 1 µm	X	✓ (impractical)	✓	✓	✓ (impractical)
PVD	High cost High layer quality	0.5-2 µm	X	✓	✓	SOA	✓
CVD	Very high cost Very thin layers	<< 1 µm	X	✓ (impractical)	✓	✓	✓ (impractical)
PLD	High cost; not scalable Thin layers Low T process	< 1 µm	X	✓	✓	SOA	✓
ESD	Low T process Large active surface Microstructure degradation at high T	5-50 µm	X	✓	✓	✓	✓
Infiltration of scaffolds	Large active surface Time-consuming Microstructure degradation at high T	-	X	SOA	X	X	SOA

2.2. Testing of single-cells

This section describes impacts of testing procedure in order to ease comparison of results and underline the importance of testing conditions. The theoretical cell voltage (electro-motoric force, EMF) of the oxidation of hydrogen at certain conditions can be calculated using the Nernst equation:

$$EMF \approx \frac{-\Delta G}{nF} = \frac{-\Delta G^0}{nF} + \frac{RT}{nF} \ln\left(\frac{p_{H_2} p_{O_2}^{1/2}}{p_{H_2O}}\right) \quad \text{(Eq. 1)}$$

Accordingly, the cell voltage directly depends on temperature and the partial pressures of the reactants at the electrodes. Hence, operating gas composition and absolute pressure substantially affect the measurement of cell performance. The cell voltage can be used to directly calculate the humidity in the fuel, which is useful to determine the amount of gas leakage in the test setup (through both cell and sealing) when using dry H_2 as fuel. Gas tightness cannot be assessed accurately when using humidified H_2 as fuel.

Gas conversion and flow rate of supplied gases (i.e. fuel utilization) play a dominant role under increasing load. This influence is even more pronounced in case of inhomogeneous gas supply over the electrode area, which therefore should be resolved generally. Moreover, the cell temperature may considerably differ from the furnace set point and can increase substantially under high current load, leading to a hysteresis in the *I-V* curve. The accuracy of the temperature measurement depends on the position of measurement as thermocouples can mostly not be placed on the cell directly.

Other important aspects for comparison of cell performance are cell dimensions and contacting of the electrodes during the measurement. Fabrication as well as contacting and gas supply are easier for small button-cells than full-sized cells suitable for stacking. To mimic ideal contacting and avoid influences due to inhomogeneous current distribution, some researchers apply noble-metal contacting pastes. However, these might also manipulate the results in either direction. For example, Ag or Pt nanoparticles exhibit pronounced activity for oxygen reduction and therefore might boost apparent performance of air electrodes.[56] In contrast, sintering of contact paste material can close open porosity of electrode structures, accompanied by hindered gas supply and lower performance. In other words, ideal contacting using all measures (such as noble metal mesh) to avoid influences of the contacting is of particular interest in fundamental scientific research focusing on reaction pathways and their individual steps. The closer applied research moves to industrialization, the more economic boundary conditions call for a solution that serves best in terms of combined cost and performance and the focus shifts to utilization of the cell performance on stack and system level.

The most well-controlled parameters for assessment of cell performance and comparison to other work are usually supplied gases, their pressure and (area specific) flow rate. Small variations in fuel humidification cause significant changes in terms of OCV at low total humidity, but tend to

alleviate under load due to gas conversion effects. In contrast, a preset water vapor content of 50 % will lead to lower power output over the whole current-voltage range in comparison to (almost) dry fuel conditions, but is relatively insensitive to humidity fluctuations. High flow rates and low fuel utilizations are applied in most single-cell characterizations in order to evaluate the performance limit of cells. Humidification is often used to assure stable output with little fluctuation but kept low for the same purpose of maximum performance. Recently, Klotz, Weber and Ivers-Tiffée recommended clear guidelines for reliable comparison of cell performance, indicating the cell voltage at a current density of 1 A cm^{-2} and pH_2O = 0.6 atm as a reliable indicator for performance comparison due to the insensitivity of these settings to humidity fluctuations, self-heating, or non-linearity.[57] Notably, the often-specified maximum power density (MPD) of an SOC is meaningless, since it not only reflects operation parameters that are irrelevant to SOC operation due to the low electrical efficiency at low cell voltages, but is also very sensitive to the testing parameters and the cell geometry.

2.3. Cells based on oxygen ion conducting electrolytes

2.3.1. Structural Design and Nomenclature

Oxygen ion conducting SOCs are named with regard to the mechanically supporting structure.[16-17] Electrolyte-supported cells (ESCs) are usually fabricated by tape casting and sintering of the electrolyte substrate and subsequent application of the electrodes. The thickness of the electrolyte tape depends on the ionic conductivity and the mechanical stability of the electrolyte material and typically ranges from 40-300 µm. Due to the relatively thick electrolyte, ESCs are predominantly operated in the higher temperature range of 750-900 °C. Moreover, the restricted thermal shock resistance limits their use to stationary applications.

The mechanical support can be provided by either of the electrodes as well. In this case, the electrolyte thickness can be reduced to less than 20 µm enabling operation at lower temperatures of 600-800 °C. Fuel electrode supported cells represent the state-of-the-art of the electrode supported design and are generally referred to as anode-supported cells (ASCs) originating from the operation in SOFC mode. ESCs and ASCs are the dominating designs used in SOC development and applications. Accordingly, these represent the cell types of commercially

available products listed in **Table 2** together with their nominal performance. Other designs use specific substrate materials differing from the functional materials of the cell. An inert support usually is a ceramic material that provides mechanical stability and sufficient open porosity for gas supply but does not participate in electrochemical or reforming reactions.[58-60] Above-mentioned designs are often referred to as fully ceramic setups, even though they comprise a cermet (e.g. Ni/YSZ) structure in the reduced state. However, fabrication and assembly are usually performed in the oxidized, and therefore fully ceramic, state (NiO/YSZ). Moreover, ceramic materials are the main constituents of each layer irrespective of the fabrication/operation status. In contrast, metal-supported cells (MSCs) utilize a porous metal for mechanical support. The intention is to make use of the ductility, superior thermal and electrical conductivity, and easy manufacturability of the metal. At the same time, thickness of more brittle ceramic or cermet layers can be kept to a minimum. This is especially attractive for use in applications that require cyclic operation and robustness against vibrations or high heating/cooling rates. Challenges arise from corrosion of the metal substrate in humid fuel conditions, interdiffusion between substrate and fuel electrode, and substantially different processing conditions required to avoid oxidation of the metal substrate. This paper focuses on fully ceramic designs. Therefore the reader is referred to MSC-specific literature for further details [29, 32, 61] and only selected examples of data on MSCs are presented hereafter.

2.3.2. Electrolytes

A variety of oxygen ion conducting materials was investigated as SOC electrolyte, establishing fluorite and perovskite-type materials as the state-of-the-art electrolytes. Among these, stabilized zirconia, doped ceria, stabilized bismuth oxides, and substituted lanthanum gallates account for the great majority of conducted experiments.

Zirconia is predominantly used in the partially or fully stabilized state, by substitution of Zr with Y (3YSZ and 8YSZ, respectively) or co-substitution with Sc and Ce (ScSZ, often simply referred to as scandia stabilized zirconia). YSZ is the material of choice in the temperature range between 700 °C and 900 °C as it provides sufficient oxygen ion conductivity and mechanical as well as chemical stability under typical operating conditions. Whereas in terms of single properties YSZ does not exhibit the best performance available, most importantly it outperforms other materials due to the absence of substantial weaknesses.[16-17] When operating the cell at 600-700 °C, ScSZ is

of interest as an alternative to YSZ due to its superior ionic conductivity.[62] However, YSZ is still used in many applications because of the higher price of Sc and issues concerning fabrication and phase stability of ScSZ.[16, 34] The largest drawback of zirconia-based electrolytes is their reactivity with Sr (and to a lesser extent La) which are elements present in many high-performance air electrodes. Formation of $SrZrO_3$ and/or $La_2Zr_2O_7$ takes place mainly during high-temperature sintering but was also evidenced after long-term exposure to relevant operating temperatures.[63-68] These zirconate phases are electrically insulating and result in an increased polarization resistance, thus lowering performance of the cell.[69] Application of diffusion barrier layers (DBLs) is commonly used to prevent or minimize the formation of detrimental reaction phases. The effectiveness of DBLs strongly depends on the processing parameters, final microstructure, and material combination. [34, 63-69]

Ceria doped with rare earth elements like Gd (GDC) or Sm (SDC) is an attractive electrolyte material because of its very high ionic conductivity.[62] However, doped ceria is prone to reduction of Ce^{4+} to Ce^{3+} when subjected to the reducing environments present in SOC fuel gas atmospheres, leading to notable electronic conductivity and performance loss due to internal short-circuiting. This issue is typically alleviated by inclusion of a pure ionic conductor to block the short-circuiting current. Apart from that, the compatibility with zirconia and conventional air electrode materials makes doped ceria an excellent choice for application as DBL.[33-34, 36]

Er stabilized Bi_2O_3 (ESB) exhibits a defective fluorite structure and provides exceptional oxygen ion conductivity at low temperature. However, even stronger reducibility than doped ceria, issues regarding phase stability, and reactivity with air electrode materials pose substantial challenges in terms of efficiency and degradation in long-term operation.[33-34, 36]

Substituted lanthanum gallate is the most common perovskite-type electrolyte material for SOC and typically applied in a $(La,Sr)(Ga,Mg)O_3$ composition providing high ionic conductivity at intermediate and low operating temperature.[70-73] A significant drawback is a pronounced reactivity with Ni and NiO, which are used in state-of-the-art fuel electrodes.[33-34, 36, 73]

Table 3 summarizes the single-cell performance of SOFCs with different electrolyte, fuel electrode, and air electrode materials. If electrochemical full-cell tests are not available, polarization resistance of the electrode materials derived from symmetrical cell measurements is

presented. Presented data is arranged according to the electrolyte materials – LSGM, ESB, stabilized zirconia, and doped ceria – and within these in the order of increasing performance with best performing material sets highlighted. As the published values usually represent initial cell performance, long-term stability and degradation behavior has to be kept in mind for evaluation of cell setups. This is another reason why YSZ is mostly chosen as the electrolyte, making use of its high reliability when using compatible electrode materials or suitable diffusion barrier layers.

The configuration with Ni/stabilized zirconia or Ni/doped ceria functional fuel electrode, stabilized zirconia electrolyte, doped ceria barrier layer, and air electrodes made of $(La,Sr)(Co,Fe)O_{3-\delta}$ or composites thereof with doped ceria today is the most common setup of oxygen ion conducting SOCs including commercial products. Within these, anode supported cells with Ni/YSZ support and thin-film electrolytes of ≤ 10 µm thickness provide the highest performance values published. As summarized in Table 3, single-cells operating at 700 °C were shown to provide current densities between 2 A cm^{-2} and 3.4 A cm^{-2} at a cell voltage of 0.7 V when optimizing design and processing, whereas more exotic materials mostly deliver inferior power output. A cross-section of a typical fuel electrode supported O^{2-}-conducting SOC is shown in **Figure 1**. To point out the difficulty to compare performance data of cells on stack level (compared to single-cell level) the influence of stacking of multiple cells is illustrated by comparing values from references [74-76] in Table 3 as one example. Whereas nominally identical cells deliver 1.7 A cm^{-2} at 0.7 V and 700 °C in single-cell measurements,[74-75] the current density reaches only 0.9 A cm^{-2} when tested in a stack,[76] as discussed in the Outlook to commercial application of SOCs. Furthermore, testing of identical cells in single-cell and stack setup and detailed analysis of the results revealed that anode polarization and contact resistance on the air side dominate the overall ASR of stacked cells of common SOCs, with minor contributions of electrolyte and air electrode.[77]

2.3.3. Fuel Electrodes

As mentioned above and can be seen from Table 3, Ni-based cermets are the most common fuel electrode material. In fact, they still are the only available electrodes with proven high performance and durability in full-cells and stacks, despite their moderate redox stability and degradation related to Ni coarsening (especially at high temperature) or Ni depletion (mostly in electrolysis mode). Ni/YSZ cermets are well-known and widely applied in SOCs. Replacing YSZ by doped ceria (GDC, SDC) aims at enhancement of catalytic activity, redox stability, and tolerance against carbon

deposition and sulfur poisoning.[33, 78-83] Formation of secondary phases with poor ionic conductivity and pores at the interface between electrolyte and fuel electrode during high-temperature sintering (> 1300 °C) impedes extensive application of ceria-based cermets in combination with stabilized zirconia electrolytes,[84] and necessitates the use of an additional ceria barrier layer between electrolyte and fuel electrode.

Investigation of fully ceramic fuel electrodes aims at development of redox tolerant cells which are less prone to poisoning by fuel impurities. In the current status of research, fully ceramic fuel electrode materials such as substituted Sr-titanates do not reach the high performance achieved with Ni-based cermets. So far, highest performance values obtained are in the range of < 1 A cm^{-2} at 700 °C (see Refs [85-90] in Table 3) corresponding to about 50 % of state-of-the-art cermets. If the performance can be enhanced to comparable levels, however, this approach shows great potential to significantly improve durability.[78, 80, 85, 90-91] One of the hot topics in SOC research is the development of electrode materials which favor exsolution of metal nanoparticles from a ceramic host matrix under reducing conditions in the fuel compartment. These embedded nanoparticles are expected to provide large active surface promoting the electrochemical reaction, at the same time being stable against agglomeration as they are pinned to the ceramic matrix.[92-94] A significant benefit is envisaged from successful implementation of such materials, as they combine the high activity of the metal surface with the superior microstructural and redox stability of ceramics.[39, 95-100] Application in full-cells and verification of sufficient stability during multiple redox-cycles including exsolution and reincorporation of the metal phase need to be addressed in further research.

2.3.4. Air Electrodes

The area of materials used as air electrode for O^{2-}-conducting SOCs is more diverse. Perovskite type materials of the formula ABO_3 represent the state-of-the-art materials. Most extensively studied are lanthanum manganites and lanthanum cobaltites, which are substituted with other elements on the A and/or B site. This substitution is used in order to improve or adapt material properties like ionic and electronic conductivity, sintering activity, thermal expansion, surface exchange, and reactivity with electrolyte materials and contaminants.[31, 101-103] The composites of $La_{1-x}Sr_xMnO_{3-\delta}$ (LSM) and stabilized zirconia used in the early generation SOCs exhibit compatibility with stabilized zirconia electrolytes but provide moderate performance as the

reaction takes place only at triple phase boundaries (see Refs [74, 104-105] in Table 3). Nonetheless, LSM/stabilized zirconia compositions are still widely used in ESCs (also see Table 2), as performance is limited by the higher resistance of the electrolyte layer. When aiming at operation below 800 °C, they were largely replaced by mixed ionic electronic conductors (MIEC) such as $La_{1-x}Sr_xCo_{1-y}Fe_yO_{3-\delta}$ (LSCF), extending the reaction zone to the entire surface of the electrode. Whereas the strontium substituted lanthanum cobaltite provides the highest electrochemical activity, the addition of Fe improves the material properties with regard to thermal expansion mismatch and stability during processing and cell operation.[17, 31, 106] High-performance materials such as the Fe free composition $La_{1-x}Sr_xCoO_{3-\delta}$ (LSC) or $Ba_{1-x}Sr_xCo_{1-y}Fe_yO_{3-\delta}$ (BSCF) enhance electrochemical performance (see Refs [74-75, 107-109]) but exhibit significantly larger coefficients of thermal expansion (CTE) and pronounced chemical expansion increasing the expansion mismatch between electrode and electrolyte.[110-113] Hence the benefit of superior electrochemical performance has to be evaluated in consideration of inferior thermo-chemo-mechanical durability. As the sites in the perovskite lattice can be occupied by various elements, there is a large number of possible element combinations and stoichiometries. Besides improving performance, substitution or addition of elements is frequently performed in order to reduce degradation phenomena. Sr tends to segregate and react with other elements. Therefore, replacing Sr is expected to improve compatibility to stabilized zirconia as well as tolerance against volatile Cr species originating from steel surfaces of interconnectors and BoP (Balance-of-Plant) or S contaminants of the supplied air.[40, 114] Segregation of Co is considered less critical, but substitution of Co might contribute to lower cost of SOCs, underlining the interest in Co free materials.[115-117] Whereas the reported performance of many Sr or Co free air electrodes is inferior compared to state-of-the-art materials, $(La,Ca)FeO_{3-\delta}$ was found to provide fast oxygen exchange [118-119] and most recently also high performance in single-cell measurements,[120] as can be seen from Table 3.

Some other perovskite types and structurally related materials have been attracting attention due to enhanced surface exchange or oxygen ion transport properties, smaller CTE mismatch, and increased tolerance against Cr species. These include the Sr free lanthanum nickelates $LaNiO_3$ and La_2NiO_4 as well as further layered perovskites of the Ruddlesden-Popper series $A_{n+1}B_nX_{3n+1}$.[31] The polarization resistances of 0.1-0.4 Ω cm² obtained at 600 °C (see Refs [121-124], Table 3) are comparable to state-of-the-art LSCF electrodes.[121-124] However, high performance was not yet demonstrated in single-cell tests. Promising performance of 1.5 A cm^{-2} at 0.7 V and 600 °C was

reported using a composite of double perovskite $YBa_{0.5}Sr_{0.5}Co_{1.75}Fe_{0.25}O_5$ and GDC as air electrode with GDC electrolyte and Ni/GDC fuel electrode.[125] Double perovskites of the composition $LnA'B_2O_{5+\delta}$ (Ln = La, Pr, Nd, Sm, Gd; A' = Ba, Sr; and B = Co, Fe, Mn) exhibit layer sequences of $A'O - BO_2 - LnO_\delta - BO_2$ which feature fast in-plane conductivity of oxygen ions in the Ln^{3+} layers.[125-126]

Dual-phase composites of an active air electrode material and electrolyte phase aim at adaptation of the coefficient of thermal expansion and/or enhancement of the ionic conductivity in the electrode. Doped ceria is commonly used as the second phase due to its compatibility with most air electrode materials. Besides the intrinsic material properties like CTE and ionic conductivity, the addition of a second phase can further change electrode properties. The sintering activity of a dual-phase composite differs from a single-phase material. For example by inhibition of particle coarsening, ceria particles affect the electrode microstructure, which fundamentally influences the electrochemical properties. Furthermore, the surface properties may change considerably due to scavenging of impurities by one of the compounds, providing a clean and highly active surface of the second phase.[31, 127-130] As a consequence, doped ceria that is generally not considered as an active material for oxygen reduction, can improve properties of air electrodes by modifying sintering behavior, microstructure, and bonding to the electrolyte. It should be noted that these implications are not universally valid but strongly depend on material combination, processing, operating conditions, and other characteristics of individual setups.

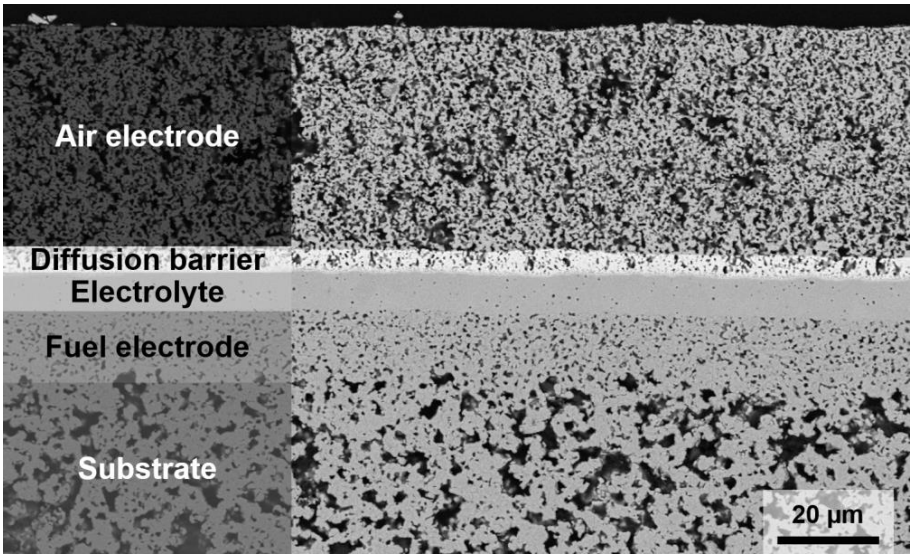

Figure 1: Cross-sectional SEM image of the microstructure of a common fuel electrode supported SOC with O^{2-}-conducting YSZ electrolyte manufactured at Forschungszentrum Jülich.

Table 2: Performance data of commercially available SOCs. Values provided on company websites or extracted from illustrations. Data of fuelcellmaterials and Elcogen single-cells derived by linear extrapolation of test results with maximum current density of 0.5 A cm^{-2} (measurement data from Elcogen AS provided by Dr Sergii Pylypko through personal communication).

Manufacturer	Type	Air electrode	Electrolyte	Fuel electrode	$j_{0.7V}$ [A cm^{-2}]	T [°C]	Reference
Kerafol	ESC	LSM/ScSZ	YSZ	Ni/YSZ	0.47	850 °C	kerafol.com
		LSM/ScSZ	YSZ	Ni/GDC	0.52		
		LSCF	ScSZ	Ni/GDC	0.88		
SOFCMAN	ESC	Not specified	ScSZ	Not specified	0.76	850 °C	sofc.com.cn
	ASC	LSCF/GDC	YSZ	Ni/YSZ	0.9	700 °C	
					≈ 0.6 (Stack)	750 °C	
fuelcellmaterials	ASC	LSC	YSZ	Ni/YSZ	0.65±0.01	600 °C	fuelcellmaterials.com
					1.1±0.05	650 °C	
					1.5±0.1	700 °C	
Elcogen	ASC	LSC	YSZ	Ni/YSZ	0.65±0.01	600 °C	Personal communication
					1.11±0.04	650 °C	
					1.6±0.1	700 °C	
					0.25 @ 0.83 V (Stack)	650 °C	elcogen.com

Table 3: Fuel cell performance of oxygen ion conducting cells (SOFCs) with different electrolyte, fuel electrode, and air electrode materials in single-cell measurements (unless noted otherwise). "-" indicates measurement of one electrode in a symmetrical cell setup. Best performing material sets highlighted for each type of electrolyte.

Air electrode	Electrolyte – barrier layer	Fuel electrode	600 °C		700 °C		Remarks	Ref.
			$j_{0.7V}$ [A cm^{-2}]	R_p [Ω cm^2]	$j_{0.7V}$ [A cm^{-2}]	R_p [Ω cm^2]		
$SrCo_{0.8}Fe_{0.2}O_3$	LSGM	$(Sr/Ba)_2FeMoO_6$			0.4-0.5	2.5-3.1	Ceramic anode	[86]
$SrCo_{0,95}Mo_{0,05}O_3$	LSGM	Ni/SDC			0.5	0.07		[131]
$SrCo_{1,5}Mo_{0,5}O_6$	LSGM	Ni/SDC			0.5	0.08		[132]
$SrCo_{0,8}Fe_{0,2}O_3$	LSGM	Sr_2MgMoO_6			0.9 (750 °C)		Ceramic anode	[87]

LSM/ESB	ESB	-		0.4				[133]
$Pr_{0.5}Ba_{0.5}MnO_3$/ESB	$Sm_{0.075}Nd_{0.075}Ce_{0.85}O_2$/ESB	Ni/ $Sm_{0.075}Nd_{0.075}Ce_{0.85}O_2$	0.7					[134]
LSM/ESB	YSZ-GDC	Ni/YSZ	0.5 (650 °C)	0.23 (650 °C)			sintering additive CuO	[104]
LSCF	*YSZ-GDC*	*$La_{0.2}Sr_{0.8}Ti_{0.9}Ni_{0.1}O_3$/ YSZ*	*0.1 (650 °C)*				*MSC, ex-solution*	*[95]*
LSM/YSZ	YSZ	$La_{0.2}Sr_{0.7}TiO_3$/GDC			0.5		Ceramic anode, T not specified	[85]
$SrFeO_3$	YSZ-SDC	Ni/YSZ	0.25	0.88	0.65			
$SrFeO_{2,95}F_{0,05}$	YSZ-SDC	Ni/YSZ	0.3	0.39	1.0			[135]
$SrFeO_{2,9}F_{0,1}$	YSZ-SDC	Ni/YSZ	0.3	0.49	0.9			
$Pr_4Ni_3O_{10+\delta}$	YSZ-GDC	Ni/YSZ		0.16 (ASR)	0.64	0.025 (ASR)		[124]
LSCF	GDC-YSZ-GDC	$Pr_{0,5}Ba_{0,5}Mn_{0,9}Mo_{0,1}O_3$			0.7 (800 °C)		Ceramic anode 800 °C	[89]
LSM/YSZ	YSZ	Ni/YSZ			0.7			[74]
$Sr_2Fe_{1,45}Sc_{0,05}Mo_{0,5}O_6$	YSZ-SDC	Ni/YSZ			0.75	0.35		[136]
LSC	*ScYSZ-GDC*	*Ni/GDC infiltrated (La,Sr)(Fe,Ni,Ti)O_3-ScYSZ-Fe22Cr*	*0.6 (650 °C)*	*0.35 (650 °C)*	*0.9*		*MSC exsolution infiltrated*	*[137]*
GDC infiltrated $La_{0.97}Ni_{0.5}Co_{0.5}O_3$	YSZ-GDC	Ni/YSZ			0.9	0.08	50 % H_2O	[138]
$PrBa_{0,7}Ca_{0,3}Co_2O_5$	YSZ-GDC	Ni/YSZ	0.4	0.16	1.1	0.035		[139]
$SrCo_{0,8}Fe_{0,1}Ga_{0,1}O_3$	YSZ-GDC	Ni/YSZ	0.5		1.3			[140]
$BaFe_{0,95}Sn_{0,05}O_3$	YSZ-SDC	Ni/YSZ	0.6		1.2	0.03	Co free	[141]
$PrBaCo_{2-x}O_{6-\delta}$	YSZ-GDC	Ni/YSZ	0.7	0.2	1 (650 °C)	0.059		[142]
$LaNi_{0,5}Co_{0,5}O_3$-GDC-YSZ	YSZ	Ni/YSZ		0.07-0.31	1.2	0.02 (air electr.)	rSOC	[143]
(PrLaBa)(FeZn)O_5/ SDC	YSZ-GDC	Ni/YSZ	0.7	0.6	1.2	0.1		[144]
LSC	YSZ-GDC	Ni/YSZ	0.7	0.5			PLD AACVD	[145]
LSM/YSZ	YSZ	Ni/YSZ			1.5 (750 °C)			[105]

$Sm_{0.5}Sr_{0.5}CoO_3$/SDC	YSZ-GDC	Ni/YSZ			1.6			[146]
LSCF	YSZ-GDC	Ni/YSZ	0.6	1.4	1.7	0.25	10 µm YSZ	[74-75]
LSCF	YSZ-GDC	Ni/YSZ	0.3		0.9	< 0.17	Stack	[76]
$La_{0,6}Ba_{0,4}CoO_3$	YSZ	-		0.17 (R_{surf})			PLD high TEC	[147]
LSC	YSZ	-		0.5			PLD	
$(Bi,Sr)(Fe,Nb)O_3$	YSZ-GDC	Ni/YSZ	0.8	0.16	2	0.04		[115]
$La_{0.65}Ca_{0.35}FeO_{3-\delta}$	YSZ-GDC	Ni/YSZ	0.6	0.65	2.1	0.21	3 µm YSZ	[120]
LSC	YSZ-GDC	Ni/YSZ	0.8		2.1		10 µm YSZ	[74]
LSCF	YSZ-GDC	Ni/YSZ	1.0	1.4	2.1	0.25	1 µm YSZ	[74-75]
$BaCo_{0.4}Fe_{0.4}Zr_{0.1}Y_{0.1}O_3$	YSZ-GDC	Ni/YSZ			2.3	0.31		[148]
Infiltrated GDC + $La_{0,95}Co_{0,4}Ni_{0,6}O_3$	YSZ (dense/ porous)	-		0.05			Low R_p in symm. cell	[149]
LSC	YSZ-GDC	Ni/YSZ	1.77				PLD	[108]
LSC	YSZ-GDC	Ni/YSZ	1.9		3.4		1 µm YSZ	[74-75]
LSC/GDC	YSZ-GDC	Ni/YSZ	2.0	0.27	2.5 (650 °C)	0.19 (650 °C)	PLD	[150]
LSCF	*GDC-YSZ-GDC*	*Ni/GDC*	*0.53 (0.75 V)*				*MSC*	*[151]*
LSC	*ScYSZ-GDC*	*Ni/GDC infiltrated Ni22Cr/YSZ*			*1.44*		*MSC*	*[107]*
LSCF	*YSZ-GDC*	*Ni/GDC*			*1.6*		*MSC*	*[152]*
Pr_6O_{11} infiltrated ScSZ	*ScSZ*	*Ni/SDC infiltrated ScSZ*			*2.2*		*MSC*	*[153]*
LSC	*YSZ-GDC*	*Ni/GDC*			*3,6*		*MSC*	*[109]*
LSM/ScSZ	ScSZ	$Gd_{0.1}Ce_{0.8}Ni_{0.1}$/ $La_{0.1}Sr_{0.9}Ti_{0.9}Ni_{0.1}O_3$			0.25 (800 °C)		exsolution	[98]
LSM/ScSZ	ScSZ	ScSZ/ $La_{0.1}Sr_{0.9}TiO_3$ + GDC + Ni/Pd			0.75-0.9 (800 °C)		Ceramic anode	[91]
LSM/YSZ	ScSZ	$La_{0,9}Ca_{0,1}Fe_{0,9}Nb_{0,1}O_{3-\delta}$/ScSZ			0.5		Ceramic anode	[88]
$Cu_{1.4}Mn_{1.6}O_4$	ScSZ	Ni/ScSZ			0.6			[154]
$La_{0,5}Sr_{0,5}Fe_{0,8}Cu_{0,15}Nb_{0,05}O_3$	ScSZ-SDC	$La_{0,5}Sr_{0,5}Fe_{0,8}Cu_{0,15}Nb_{0,05}O_3$			1 (800 °C)	0.16 (800 °C)	Cu exsolution	[99]
$Pr_{0.5}Sr_{0.5}Cu_{0.2}Fe_{0.8}O_3$	ScSZ-SDC	$La_{0,5}Sr_{0,5}Fe_{0,8}Cu_{0,1}Ti_{0,1}O_3$			0.8	0.26	Ceramic anode	[90]

-	SDC	$La_{0,4}Sr_{0,4}Sc_{0,9}Ni_{0,1}O_3$/ SDC				0.25	exsolution	[96]
Infiltrated $CuCo_2O_4$	ScSZ	Not specified			1			[155]
$Sr_{0,95}Co_{0,7}Nb_{0,1}Fe_{0,2}O_3$	SDC	Ni/SDC	0.05	0.43	0.1	0.11		[156]
$La_2NiO_{4+\delta}$	GDC	-		0.42		0.08	ESD	[122]
$La_3Ni_2O_7$/GDC	GDC	-		0.13		0.03		[121]
$NdBa_{0,96}Co_2O_5$	SDC	(Ni,Cu)/SDC			< 0.25 (650 °C)	0.3 (650 °C)		[126]
LSCF/GDC	GDC	$Sr_{0,2}Na_{0,8}Nb_{0,9}V_{0,1}O_3$/ GDC			0.25 (650 °C)	0.2 (650 °C)	Ni free	[157]
$LaPrNiO_4$	GDC	Ni/YSZ	0.25	0.12	0.5		ESD	[123]
LSCF/GDC	GDC	Ni/GDC	0.4	0.17				[158]
CuO infiltrated LSCF	SDC	Ni/SDC	0.4					[159]
LSCF/GDC	GDC	-		0.07			ESD	[160]
LSCF	GDC	-		0.07		0.02 (650 °C)	ESD	[52]
$YBa_{0,5}Sr_{0,5}Co_{1,75}Fe_{0,25}O_5$/GDC	GDC	Ni/GDC	1.5	0.08				[125]

2.3.5. Solid Oxide Electrolysis Cells

Data of investigations in electrolysis mode is sparse in comparison to fuel cell mode, as can be seen from **Table 4**. Electrolysis is considered increasingly important driven by economic and environmental issues. Countries that have limited access to fossil resources like Japan or South-Korea push the development of a hydrogen society in order to become more independent in terms of energy supply. At the same time, large efforts are placed on a climate-neutral economy as specified in the Paris Agreement and the European Green Deal of the EU.[161-162] Therefore, performance and degradation phenomena of cells operated in SOEC mode, have been investigated in more detail recently. The materials used for fabrication of the functional layers are similar to traditional SOFC materials as these exhibit catalytic activity in both operational modes and often provide initial SOEC performance in agreement with SOFC tests. However, comparison of the available data is complicated by a lack of standardized operation conditions. The operating temperature in electrolysis mode is mostly between 700 °C and 850 °C, which is higher than the

average fuel cell operating temperature. The operation can be categorized in pure H_2O electrolysis, pure CO_2 electrolysis and co-electrolysis of H_2O and CO_2.[25, 163] Furthermore, the H_2/H_2O ratio of the fuel composition differs in literature due to different amounts of H_2 fed. This can be because of limitations of the experimental setups or in order to ensure a sufficiently reducing atmosphere. Published data also differ in the cell voltage or current density used for comparison of performance. Most applications aim at operation close to the thermo-neutral point, resulting in a cell voltage around 1.3 V. At this operating point, the net reaction heat and Joule heating of the cell level out, minimizing the required external heating or cooling.[25]

Whereas the initial performance of SOEC mostly is in accordance with SOFC performance, degradation was found to be substantially different when cells are operated in electrolysis mode. In addition to well-known degradation caused by fuel impurities or contaminants, SOEC-specific degradation phenomena occur. Among these, crack formation in the electrolyte or at the electrolyte/air electrode interface, Ni migration leading to depletion of Ni at the electrolyte/fuel electrode interface, and carbon deposition at the fuel electrode when operating on carbon-containing fuel are considered most critical. High current densities and increased polarizations of electrodes and interfaces at higher cell voltage increase degradation rates. Furthermore, the redox reactions at the air and fuel electrode are reversed in comparison to fuel cell operation, which might affect the degree of degradation processes. Crack formation on the air side is hypothesized to occur due to high vapor pressure of oxygen in the electrolyte or at the interface to the electrode. Materials and microstructures with improved transport properties and fast oxygen evolution are desired to improve durability. Improved long-term stability was achieved by interface engineering [164] and optimization of the electrode microstructure and composition.[165-167] Carbon deposition can be mitigated by monitoring the gas composition and ensuring sufficient water vapor content.[168] Moreover, new materials are investigated that are less prone to carbon deposition than pure Ni. Examples are Ni-Sn [169] and Ni-Cu alloys or incorporation of Mo in the fuel electrode structure.[170] However, the addition of foreign elements frequently decreases cell performance and processing is complicated due to the low melting point of the alloying elements and limited solubility at high temperature.[170-172]

A deeper understanding of Ni migration is crucial for further SOEC development. Early hypotheses regarding the mechanism of Ni migration were based on evaporation of Ni species in highly humid

atmospheres.[173] However, Ni migration does not occur under OCV conditions which present the highest humidity but only under polarization.[174] Comparison of stack test data [175-176] and FactSage calculations of the vapor pressure of Ni species at 800 °C in a typical 90 % H_2O, 10 % H_2 atmosphere indicate that evaporation is unlikely to be the sole reason for Ni migration. $Ni(OH)_2$ exhibits the highest vapor pressure of $1.8 \cdot 10^{-10}$ bar. Considering 18000 h of stack operation and the amount of gas fed to the fuel electrode, only 0.25 % of the Ni in the functional layer can be evaporated. Therefore, polarization-dependent properties of the fuel electrode cermet are expected to play a key role in Ni migration. This is in agreement with published results indicating enhanced durability achieved by minimization of the electrode overpotential due to optimized processing [177] and observation of polarization-dependent wettability of Ni in contact with YSZ.[178-179] Based on these findings, Trini et al. [180] hypothesized that the reverse effect of Ni loss due to Migration observed during electrolysis operation is likely to occur after very long operation in fuel cell mode, leading to Ni enrichment in the fuel electrode. This assumption was recently supported in a publication of Menzler et al. on the results of the post-test analysis of an SOFC stack operated for 100.000 h at 700°C.[181]

Table 4: Electrolysis performance of oxygen ion conducting cells (SOECs) with different electrolyte, fuel electrode, and air electrode materials in single-cell measurements (unless noted otherwise). Best performing material sets highlighted.

Air electrode	Electrolyte – barrier layer	Fuel electrode	700 °C		800 °C		Remarks	Ref.
			j [A cm^{-2}]	R_p [Ω cm^2]	j [A cm^{-2}]	R_p [Ω cm^2]		
$La_{0.6}Sr_{0.4}Fe_{0.8}Mn_{0.2}O_3$	LSGM	$Ba_{0.6}La_{0.4}CoO_3$			0.52 @ 1.6 V (900 °C)			[182]
Ni, Cu, Ni/Cu infiltrated $La_{0.75}Sr_{0.25}Cr_{0.5}Mn_{0.5}O_3$ /SDC	LSGM	LSM/SDC			0.28 @ 1.2 V (CO_2)	0.75-3		[183]
$Bi_{0,42}Y_{0,58}O_{1,5}$/LSM	YSZ	Ni/YSZ		0.25				[184]
-	YSZ dense/porous	LSM				0.5		[164]
LSC/GDC	YSZ-GDC	Ni/YSZ		0.15 (750 °C)				[165]
$La_{0.8}Sr_{0.2}Co_{0.8}Ni_{0.2}O_3$ infiltrated LSM/GDC	YSZ	Ni/YSZ			0.8 @ 1.2 V	0.12		[185]
LSC infiltrated LSCF	YSZ-GDC	Ni/YSZ			0.7 @ 1.1 V	0.06		[167]
LSC infiltrated GDC	YSZ-GDC	Ni/YSZ	0.3 @ 1.1 V	0.18	0.8 @ 1.1 V	0.09		[186]
LSCF	YSZ-GDC	Ni/YSZ	0.3 @ 1.1 V	< 0.17	0.75 @ 1.1 V	< 0.1	Stack	[76]
LSC/GDC	YSZ-GDC	Ni/YSZ			1 @ 1.1 V	0.14		[177]
Pr_6O_{11} infiltrated ScSZ	*ScSZ*	*Ni/SDC infiltrated ScSZ*	*1.0 @ 1.1 V*		*2.4 @ 1.1 V*		*MSC*	*[187]*

2.4. Cells based on proton conducting electrolytes

Proton conducting materials exhibit promising properties for use as SOC electrolyte. Proton conduction is comparably fast at low and intermediate temperatures of 350-550 °C, making proton conducting fuel cells (PCFCs) attractive for low-temperature operation. Moreover, very high fuel utilization and operation at peak power are possible as water is formed at the air side and the fuel is not diluted by water vapor, maintaining safe conditions for redox prone fuel electrodes. However, achieving sufficient conductivity in the range of 10^{-2} S cm^{-1} is challenging at temperatures above 500 °C as dehydration of the material leads to decrease of the charge carrier concentration.

2.4.1. Electrolytes

Acceptor doped $BaZrO_3$-$BaCeO_3$ solid solutions are the basis for most PCFC electrolytes. Barium zirconate exhibits high phase stability and chemical stability in typical SOC fuel atmospheres containing H_2O, CO_2, CO, CH_4, and H_2S but shows limited proton conductivity due to pronounced blocking effects of grain boundaries.[188] In contrast, barium cerates provide very high conductivity, a coarser microstructure with fewer grain boundaries, and high charge carrier concentration but insufficient thermochemical stability during operation. The higher reducibility of $BaCeO_3$ compared to $BaZrO_3$ and reactivity with CO_2 and H_2O to form carbonates or hydroxides prevent the use of pure $BaCeO_3$ as electrolyte for proton conducting SOC. The combination of both systems provides an electrolyte material with high conductivity and sufficient stability.[188-189] Y is the most common dopant and frequently combined with Yb doping in order to enhance conductivity and catalytic reforming of hydrocarbons. The resulting $Ba(Zr,Ce,Y,Yb)O_{3-\delta}$ (BZCYYb) electrolyte compositions exhibit conductivities in the range of 10^{-2} S cm^{-1} at 600 °C and improved coking resistance.[190-191] Nonetheless, stability in atmospheres containing water vapor, CO_2 or hydrocarbons remains an issue.[189, 192] Densification of the electrolyte layer is often reported to present another difficulty. Very high temperatures of > 1600 °C required for densification of single-phase $BaZrO_3$ compositions are in conflict with the requirement of high porosity of electrode substrates, and cause loss of Ba due to evaporation, negatively affecting the proton conductivity. A widespread approach to densify $BaZrO_3$-$BaCeO_3$ mixtures at lower sintering temperature is the addition of suitable amounts of sintering aids such as CuO, NiO, ZnO, and Bi_2O_3 while keeping high proton conductivity.[189] However, it was recently reported that co-sintering of the electrolyte on an electrode substrate can promote densification and provide sufficiently dense electrolyte layers even at temperatures as low as 1350 °C.[193] This phenomenon is actually not novel but well-known from fabrication of SOFC (YSZ electrolyte on Ni/YSZ substrate). The higher shrinkage of the support presents an additional driving force for electrolyte sintering due to compressive stresses, thereby enhancing densification.[194-195]

Other materials investigated as PCFC electrolyte suffer from insufficient proton conductivity at relevant operating temperature. Lanthanum tungstate presents an alternative to the $Ba(Zr,Ce,Y,Yb)O_{3-\delta}$ materials if very thin films of about 1 µm thickness can be manufactured. High thermochemical stability, better sinterability, and less blocking effects of the grain boundaries

are advantageous for application as electrolyte, while the conductivity is about one order of magnitude lower than the one of $BaZrO_3$-$BaCeO_3$ compositions at 800 °C.[196-198]

2.4.2. Fuel Electrodes

Similar to cells based on oxygen ion conductors, PCFC fuel electrodes are usually cermets made of electrolyte material and NiO, which is reduced to metallic Ni when subjected to fuel conditions at the beginning of operation.[199-200] The microstructure of a representative fuel electrode supported PCFC is shown in **Figure 2**. Symmetrical cells using other materials such as $BaFeMo_2O_6$ as fuel electrode did not yet achieve performance comparable to Ni/electrolyte cermets.[201]

2.4.3. Air Electrodes

Air electrode materials used for SOFCs are widely applied also as PCFC air electrode and frequently mixed with electrolyte material to form a dual-phase electrode. Addition of the electrolyte phase improves the proton conductivity and extends the available reaction zone, similar to early LSM/YSZ air electrodes for SOFC.[202-204] The pronounced MIEC properties and fast surface exchange are beneficial for both SOFC and PCFC. However, state-of-the-art SOFC air electrodes like LSCF show negligible proton conductivity at relevant operating temperature [205] and many proton conducting materials suffer from dehydration at temperatures above 400 °C. Therefore, development of air electrode materials with enhanced hydration properties and improved stability of protons at elevated temperature is desired. Of special interest are triple conducting materials (e^-, O^{2-}, H^+) in order to maximize the reaction zone and active volume of air electrodes.[189, 206-208] Proton conducting air electrode materials usually limit the possible sintering temperature to 800-1000 °C increasing the risk of delamination due to poor contact with the electrolyte and stresses induced by CTE mismatch.[209] Some of the most promising air electrode materials reported are double-perovskites of the composition $LnA'B_2O_{5+\delta}$ (Ln = La, Pr, Nd, Sm, Gd; A' = Ba, Sr; and B = Co, Fe, Mn).[210-211] **Table 5** summarizes performance of various PCFCs reported in literature. Most single-cell measurements show moderate performance of 0.4-0.6 A cm^{-2} at 0.7 V and 600 °C.[212-214] Substantial performance enhancement to 1.4 A cm^{-2} at 0.7 V and 600 °C was achieved using a $PrBa_{0.5}Sr_{0.5}Co_{1.5}Fe_{0.5}O_{5+\delta}$ (PBSCF) air electrode providing enhanced solubility of protons. A dense PBSCF interlayer applied by PVD on the $BaZr_{0.4}Ce_{0.4}Y_{0.1}Yb_{0.1}O_3$ electrolyte is reported to enhance contact between electrode and

electrolyte.[206] High performance of 1.75 A cm^{-2} was reported using a cell comprising of thin (< 5 µm) BZCY electrolyte fabricated on a co-shrinking Ni/BZCY substrate and BSCF air electrode.[193] Further progress in terms of performance and durability is envisaged by application of advanced PCFC air electrode materials. Certainly, extended durability (stack) tests are required to evaluate the industrial applicability of PCFCs. Relevant lifetimes cover at least 8,000 h (1 year) of operation in order to become commercially viable, and more likely should last several 10,000 h in stationary applications. The available single-cell test durations of up to 1,400 h [192, 206, 215-216] illustrate the gap in maturity of PCFC technology in comparison to SOFC.

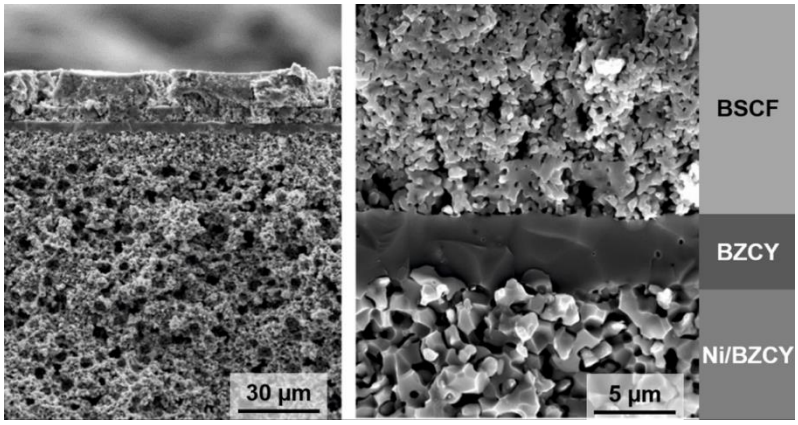

Figure 2: Cross-sectional SEM image of the microstructure of a high-performance fuel electrode supported proton conducting cell. Adapted by permission from Springer Nature.[193]

Table 5: Fuel cell performance of PCFCs with different electrolyte, fuel electrode, and air electrode materials in single-cell measurements. Best performing material sets highlighted.

Air electrode	Electrolyte	Fuel electrode	600 °C		700 °C		Remarks	Ref.
			$j_{0.7V}$ [A cm^{-2}]	R_p [Ω cm^2]	$j_{0.7V}$ [A cm^{-2}]	R_p [Ω cm^2]		
$PrBaCo_2O_5$/ $Ba(Zr,Ce,Y,Yb)O_3$ (BZCY)	BZCY $BaZr_{0,3}Ce_{0,5}Y_{0,2}O_3$	Ni/BZCY	P_{max} 0.27 W cm^{-2}		P_{max} 0.67 W cm^{-2}		Bi_2O_3 sintering aid	[217]
$La_3Ni_{1,6}Co_{0,4}O_7$	BZCY	Ni/BZCY	0.3	0.35 (650 °C)	0.5			[218]
LSCF/BZCYYb	BZCYYb	Ni/BZCYYb	0.4		0.5			[219]
$LiNi_{0,8}Co_{0,2}O_2$/BZCY	BZCY	Ni/BZCY	0.5 (650 °C)				ZnO sintering aid	[207]
$(Pr,La)(Ni,Cu,Nb)O_4$ infiltrated BZCY	BZCY	Ni/BZCY	0.4		0.7			[212]
$PrBaCo_2O_5$/BZCYYb	BZCYYb + Co	Ni/BZCYYb	0.4	0.35	0.7	0.12		[220]
$SmBaCo_2O_5$/SDC	$BaCe_{0,8}Y_{0,15}Nd_{0,05}O_3$	Ni/ $BaCe_{0,8}Y_{0,15}Nd_{0,05}O_3$	0.4	0.3	0.7	0.08		[213]
$Sm_{0.5}Sr_{0.5}CoO_3$ infiltrated GDC	BZCYYb	Ni/BZCYYb	0.6		0.7			[214]
$BaCo_{0.4}Fe_{0.4}Zr_{0.1}Y_{0.1}O_3$	BZCYYb	Ni/BZCYYb	0.9				0.6 A cm^{-2} (500 °C)	[192]
$PrBa_{0,5}Sr_{0,5}Co_{1,5}Fe_{0,5}O_5$	BZCYYb	Ni/BZCYYb	1.1	0.14			Without PLD	[206]
$PrBa_{0,5}Sr_{0,5}Co_{1,5}Fe_{0,5}O_5$	BZCYYb	Ni/BZCYYb	1.4	0.14			+ PLD	[206]
$Ba_{0,5}Sr_{0,5}Co_{0.8}Fe_{0.2}O_{3-\delta}$	BZCY	Ni/BZCY	1.75	0.09			< 5 µm electrolyte 1350 °C sintered	[193]

2.4.4. Proton Conducting Electrolysis Cells

Operation of proton conducting cells in electrolysis mode (PCEC) was reported to result in substantially lower efficiency than fuel cell operation.[215] Therefore, little data on PCEC is available. Recently, it was shown that BZCYYb compositions show drastically improved PCEC performance due to lower electronic leakage compared to BZY-type materials, reaching between 0.75 A cm^{-2} and 1.92 A cm^{-2} at 1.3 V and 600 °C (3-20 % H_2O),[215-216, 221-222] as shown in **Table 6**. Despite these improvements, significant contributions of electronic leakage may still reduce the efficiency of electricity to hydrogen conversion. Moreover, the performance in electrolysis mode cannot be directly extracted from the *I-V*-curve, contrary to fuel cell operation. In both operational

modes, an internal electronic leakage decreases the cell voltage. In fuel cell mode, this directly corresponds to lower performance. In electrolysis, however, a lower voltage at given current indicates an improved performance assuming constant conversion efficiency. It is therefore important, to include the Faradaic efficiency (FE), which describes the ratio of produced amount of hydrogen to the theoretical amount assuming full conversion. Otherwise, the provided data only describe the power input without indication of product output. Whereas in some works values up to 98 % were obtained,[215] others obtained lower FE of 76 %.[216]

Table 6: Electrolysis performance of PCECs with different electrolyte, fuel electrode, and air electrode materials in single-cell measurements.

Air electrode	Electrolyte	Fuel electrode	550 °C		600 °C		Remarks	Ref.
			$j_{1.3V}$ [A cm^{-2}]	R_p [Ω cm^2]	$j_{1.3V}$ [A cm^{-2}]	R_p [Ω cm^2]		
$NdBa_{0,5}Sr_{0,5}Co_{1,5}Fe_{0,5}O_5$ /BZCYYb	BZCYYb	Ni/BZCYYb	0.42	0.38	0.75	0.21	"Hybrid"-cell 10 % H_2O in H_2 and air; FE not given	[221]
$PrBa_{0,5}Sr_{0,5}Co_{2-x}Fe_xO_5$	BZCYYb	Ni/BZCYYb	0.42		0.85		95Ar/5H_2 12 % H_2O in O_2; FE > 97 % (500 °C)	[222]
$BaCo_{0.4}Fe_{0.4}Zr_{0.1}Y_{0.1}O_3$	BZCYYb	Ni/BZCYYb	0.75	≈ 0.17	1.0	≈ 0.14	10-85 % H_2O in N_2; FE > 90 %	[215]
$PrBa_{0,5}Sr_{0,5}Co_{1,5}Fe_{0,5}O_5$	BZCYYb	Ni/BZCYYb	0.75	0.25	1.42	0.14	Without PLD; FE 74-87 %	[216]
			1.0	0.28	1.92	0.15	+ PLD; FE 74-87 %	

3. Conclusion

Many novel materials have been investigated for application in SOC. Promising characteristics of these newly developed materials were mainly obtained in symmetrical cell setups, as they enable easy fabrication and testing. However, the validation of high performance in full-cell tests either was not yet addressed or did not provide the intended benefit. In parallel, setups utilizing traditional material combinations were optimized as well, thus still providing the highest power output published (see **Figure 3**). Current densities of 2.0-3.4 A cm^{-2} at 0.7 V and 700 °C are reported for

state-of-the-art cells consisting of Ni/YSZ substrate and fuel electrode, YSZ electrolyte, GDC diffusion barrier, and air electrodes made of (La,Sr)(Co,Fe)$O_{3-\delta}$ or dual-phase composites thereof with doped ceria. This emphasizes the importance of microstructure, processing, and combined properties of the applied materials. Whereas 700-800 °C is a quite common range of SOC (ESC/ASC) operating temperature at which traditional materials show beneficial properties, different material combinations or processing techniques can be advantageous when the intended application and operation conditions change. Especially for low-temperature operation, highly active electrode structures with large active surface and low interfacial resistance to the electrolyte are crucial. For this, suitable processing needs to be combined with long-term stability at operating temperature. High-temperature exposure should be kept to a minimum to avoid loss of active surface by coarsening. Advanced processing techniques like PVD and PLD can provide high-quality layers with adjustable microstructure providing enhanced performance. However, industrial application is impeded by their higher cost and limited scalability.

Large improvements were achieved with regard to the development of high-performance air electrode materials, which presented the bottleneck in early-stage research. This, in turn, opens the possibility to exploit the potential of enhanced fuel electrodes in further activities. Application of doped ceria in fuel electrodes is of high interest for two reasons. Firstly, the electrochemical activity of ceria under fuel conditions contributes to enhanced cell performance. Secondly, Ni/doped ceria cermets show potential for increased stability in SOEC mode due to reduced electrode overpotential. An issue to be solved for widespread application of ceria-based fuel electrodes is their processing in contact with a YSZ electrolyte, as interdiffusion leads to pore formation at the interface and increased ohmic resistance. Doped ceria is highly relevant also as an electrolyte material when aiming at low operating temperature. Here, effective measures need to be established to avoid electronic leakage, e.g. by application of blocking layers. If successfully realized, doped ceria electrolytes may contribute substantially to enhanced low-temperature performance.

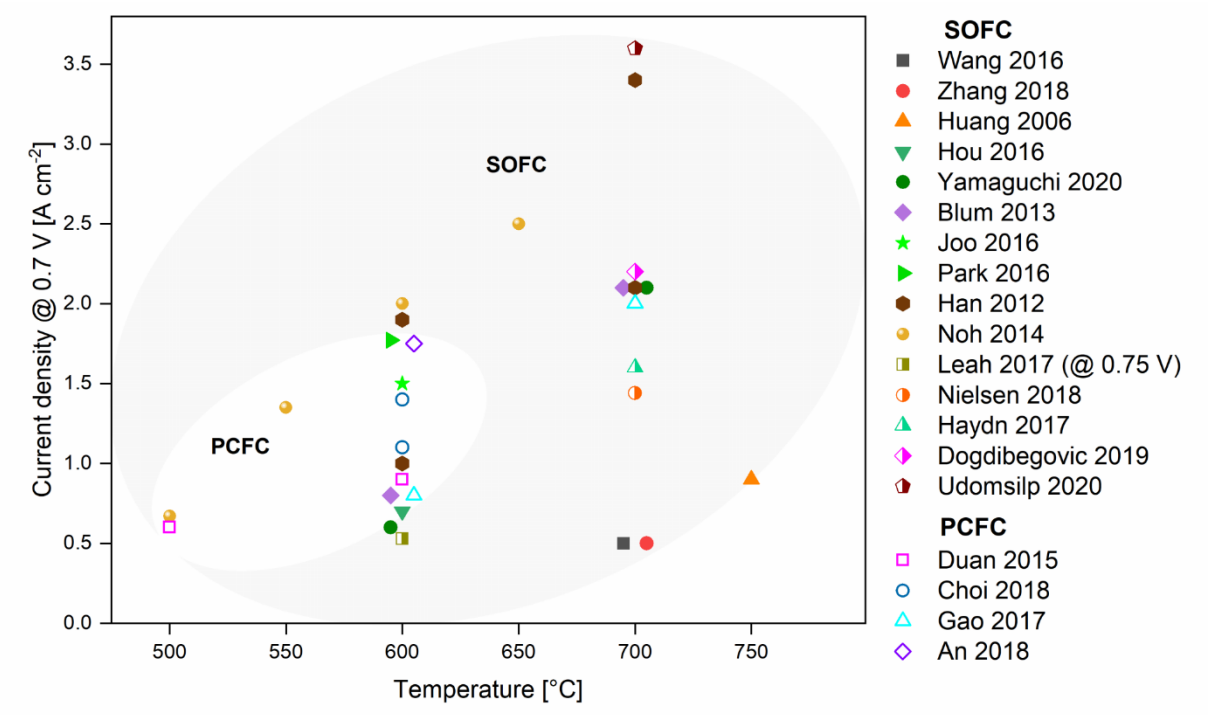

Figure 3: Current density of selected SOFC (closed symbols; MSC – half-filled symbols) and PCFC (open symbols) achieved in single-cell tests.

Great potential is attributed to PCFCs when aiming at low-temperature operation. Very promising properties were identified in early-stage research but considerable improvement is still required to effectively compete with existing SOFC designs. Here, the development of better air electrodes exhibiting adequate proton conductivity at operating temperature is especially important, together with evaluation of long-term stability (>> 1,000 h), scale-up, and stack testing.

In summary, it becomes clear that the choice of cell type, design, materials, and fabrication techniques strongly depends on the intended application. Operating temperature, the fuel to be used, desired lifetime, thermal as well as redox cyclability, and of course cost and performance targets have to be considered in order to select the optimum cell type. From this, it can be deduced, that the future SOC technology will not be represented by a single *state-of-the-art* cell covering all sorts of applications, but more likely will consist of customized designs serving particular operating conditions. The data on cell performance, material properties and manufacturing presented in this article provide a basis for goal-oriented development in academic research as well as a guideline for industrial considerations.

Outlook to commercial application of SOCs. For successful commercialization of SOCs, the single-cell performance and durability is only the first step of development. As a single cell only provides a voltage of about 1 V, several cells need to be connected to form a stack, meeting industrial requirements with regard to power output. Some fundamental differences and limitations have to be considered when operating SOCs in a stack in comparison to the single-cell characteristics. Reliable mechanical integration, sealing, electrical contact, and gas supply are examples for basic considerations in stack design. All of these factors contribute to losses and affect durability in stack operation to individual extent. Stacking of cells introduces additional interfaces between cells, interconnectors, barrier layers, and contact layers. These interfaces present extra barriers for current flow and therefore cause contact resistances. Another challenge is a homogeneous gas distribution between the layers as well as within each cell. A three-dimensional temperature distribution with a mean stack temperature rather than a homogeneous temperature at every active site causes different reaction rates, local fuel utilizations, and thermal stresses which complicate stack operation. Furthermore, characterization of small single-cells is often performed with rather small fuel utilization, whereas stack operation aims at high fuel utilization in order to efficiently exploit the chemical energy of the fuel. As a result, cells assembled in a stack generally do not deliver the same power output as an identical cell tested in single-cell operation. To illustrate the magnitude of this issue, recent results show that the current output of a high-performance cell in a Jülich F10 stack is only about 50 % of the current measured on identical cells in a single cell test, at 700 °C and a cell voltage of 0.8 V.

Also, degradation behavior is likely to differ between ideal lab conditions of single-cell testing and real stack operation. This is due to contaminants of fuels (S- or C-containing species) and air (CO_2, H_2O, S, Cr), different operating conditions, or inhomogeneous gas- and temperature-distribution to name just a few causes. Consequently, the job is not done after optimization of single materials, but tests in real stacks or stack-mimicking environments (e.g. Cr-containing interconnector material) are crucial parts of material development. Subsequently, stack and system development are another important topic on the way to widespread application of SOCs.

Conflicts of interest

There are no conflicts of interest to declare.

Acknowledgements

The authors would like to thank Dr M. Ivanova for in-depth scientific discussion and all current and former co-workers for their contribution to SOC development at the Institute of Energy and Climate Research, IEK-1: Materials Synthesis and Processing.

Author Contributions

Conceptualization: N.H.M. and D.U.; Investigation: D.U., C.L. and N.H.M.; Writing – Original Draft: D.U.; Writing – Review & Editing: C.L., N.H.M. and O.G.; Visualization: D.U.; Supervision: N.H.M.; Project Administration: N.H.M.;

References

[1] IEA, *CO2 Emissions from Fuel Combustion 2018*, **2018**, access: 2019/07/24, https://webstore.iea.org/download/direct/2373?filename=co2_emissions_from_fuel_combustion_2018_highlights.pdf

[2] V. Lawlor, M. Reissig, J. Makinson, J. Rechberger, *ECS Transactions* **2017**, *78*, 191.

[3] J. Rechberger, M. Reissig, V. Lawlor, Springer Fachmedien Wiesbaden, Wiesbaden, **2018**, pp. 51.

[4] L. Nissan Motors Co., *Press release - range extender*, **2016**, access: 01.09.2017, https://newsroom.nissan-global.com/releases/release-3e21870a4078f6ae6a08693da300e19f-160614-01-e?year=2016&month=6

[5] A. Ballard, T. Domanski, L. Rees, C. Nobbs, N. Lawrence, K. Heffer, J. Harman, C. Evans, P. Barnard, S. Mukerjee, M. Selby, *ECS Transactions* **2019**, *91*, 117.

[6] C. Geipel, K. Hauptmeier, K. Herbrig, F. Mittmann, M. Münch, M. Pötschke, L. Reichel, T. Strohbach, T. Seidel, A. Surrey, C. Walter, *ECS Transactions* **2019**, *91*, 123.

[7] R. Küngas, P. Blennow, T. Heiredal-Clausen, T. Holt Nørby, J. Rass-Hansen, J. B. Hansen, P. G. Moses, *ECS Transactions* **2019**, *91*, 215.

[8] A. Mai, J. G. Grolig, M. Dold, F. Vandercruysse, R. Denzler, B. Schindler, A. Schuler, *ECS Transactions* **2019**, *91*, 63.

[9] M. Noponen, P. Torri, J. Göös, J. Puranen, H. Kaar, S. Pylypko, M. Roostar, E. Õunpuu, *ECS Transactions* **2019**, *91*, 91.

[10] O. Posdziech, T. Geißler, K. Schwarze, R. Blumentritt, *ECS Transactions* **2019**, *91*, 2537.

[11] D. Hara, *ECS Transactions* **2019**, *91*, 3.

[12] T. Nakao, S. Inoue, S. Uenoyama, Y. Takuwa, M. Suzuki, *ECS Transactions* **2019**, *91*, 43.

[13] R. A. George, *Journal of Power Sources* **2000**, *86*, 134.

[14] S. C. Singhal, *High temperature solid oxide fuel cells : fundamentals, design and applications*, Elsevier, Oxford, **2003**.

[15] S. C. Singhal, *Solid State Ionics* **2002**, *152–153*, 405.

[16] D. J. L. Brett, A. Atkinson, N. P. Brandon, S. J. Skinner, *Chemical Society Reviews* **2008**, *37*, 1568.

[17] N. H. Menzler, F. Tietz, S. Uhlenbruck, H. Buchkremer, D. Stöver, *J Mater Sci* **2010**, *45*, 3109.

[18] T. Li, T. M. M. Heenan, M. F. Rabuni, B. Wang, N. M. Farandos, G. H. Kelsall, D. Matras, C. Tan, X. Lu, S. D. M. Jacques, D. J. L. Brett, P. R. Shearing, M. Di Michiel, A. M. Beale, A. Vamvakeros, K. Li, *Nature Communications* **2019**, *10*, 1497.

[19] N. Russner, S. Dierickx, A. Weber, R. Reimert, E. Ivers-Tiffée, *Journal of Power Sources* **2020**, *451*, 227552.

[20] E. Achenbach, *Journal of Power Sources* **1994**, *49*, 333.

[21] Z. Gao, L. V. Mogni, E. C. Miller, J. G. Railsback, S. A. Barnett, *Energy & Environmental Science* **2016**, *9*, 1602.

[22] C. Graves, S. D. Ebbesen, M. Mogensen, K. S. Lackner, *Renewable and Sustainable Energy Reviews* **2011**, *15*, 1.

[23] O. Guillon, A. Dash, C. Lenser, S. Uhlenbruck, G. Mauer, *Advanced Engineering Materials*, *n/a*, 2000529.
[24] C. M. Harrison, P. R. Slater, R. Steinberger-Wilckens, *Solid State Ionics* **2020**, *354*, 115410.
[25] A. Hauch, R. Küngas, P. Blennow, A. B. Hansen, J. B. Hansen, B. V. Mathiesen, M. B. Mogensen, *Science* **2020**, *370*, eaba6118.
[26] S. P. Jiang, *Materials Science and Engineering: A* **2006**, *418*, 199.
[27] M. B. Mogensen, M. Chen, H. L. Frandsen, C. Graves, J. B. Hansen, K. V. Hansen, A. Hauch, T. Jacobsen, S. H. Jensen, T. L. Skafte, X. Sun, *Clean Energy* **2019**, *3*, 175.
[28] F. Wang, H. Kishimoto, T. Ishiyama, K. Develos-Bagarinao, K. Yamaji, T. Horita, H. Yokokawa, *Journal of Power Sources* **2020**, *478*, 228763.
[29] V. V. Krishnan, *Wiley Interdisciplinary Reviews: Energy and Environment* **2017**.
[30] A. B. Stambouli, E. Traversa, *Renewable and Sustainable Energy Reviews* **2002**, *6*, 433.
[31] C. Sun, R. Hui, J. Roller, *J Solid State Electrochem* **2010**, *14*, 1125.
[32] M. C. Tucker, *Journal of Power Sources* **2010**, *195*, 4570.
[33] S. P. S. Badwal, F. T. Ciacchi, *Ionics* **2000**, *6*, 1.
[34] J. W. Fergus, *Journal of Power Sources* **2006**, *162*, 30.
[35] H. Inaba, H. Tagawa, *Solid State Ionics* **1996**, *83*, 1.
[36] V. V. Kharton, F. M. B. Marques, A. Atkinson, *Solid State Ionics* **2004**, *174*, 135.
[37] E. D. Wachsman, K. T. Lee, *Science* **2011**, *334*, 935.
[38] Y. Zhang, R. Knibbe, J. Sunarso, Y. Zhong, W. Zhou, Z. Shao, Z. Zhu, *Advanced Materials* **2017**, 1700132.
[39] A. Atkinson, S. Barnett, R. J. Gorte, J. T. S. Irvine, A. J. McEvoy, M. Mogensen, S. C. Singhal, J. Vohs, *Nature Materials* **2004**, *3*, 17.
[40] H. Yokokawa, H. Tu, B. Iwanschitz, A. Mai, *Journal of Power Sources* **2008**, *182*, 400.
[41] J. B. Goodenough, K. Huang, *Solid oxide fuel cell technology : principles, performance and operations*, Woodhead Publ., Oxford, **2009**.
[42] N. Christiansen, J. B. Hansen, H. Holm-Larsen, M. Juel Jørgensen, M. Wandel, P. Vang Hendriksen, A. Hagen, S. Ramousse, *ECS Transactions* **2009**, *25*, 133.
[43] N. Christiansen, J. B. Hansen, H. H. Larsen, S. Linderoth, P. H. Larsen, P. V. Hendriksen, A. Hagen, *ECS Transactions* **2007**, *7*, 31.
[44] M. Noponen, P. Torri, J. Göös, D. Chade, P. Hallanoro, A. Temmo, A. Koit, E. Ounpuu, *ECS Transactions* **2015**, *68*, 151.
[45] S. Aruliah, S. Amarasinghe, J. Love, R. Ratnaraj, A. Summergreene, M. Watts, *ECS Transactions* **2007**, *7*, 51.
[46] O. Kesler, M. Cuglietta, J. Harris, J. Kuhn, M. Marr, C. Metcalfe, *ECS Transactions* **2013**, *57*, 491.
[47] R. Nédélec, S. Uhlenbruck, D. Sebold, V. A. C. Haanappel, H. P. Buchkremer, D. Stöver, *Journal of Power Sources* **2012**, *205*, 157.
[48] S. Vieweger, R. Mücke, N. H. Menzler, H. P. Buchkremer, *Fuel Cells* **2013**, *13*, 556.
[49] T. Z. Sholklapper, H. Kurokawa, C. P. Jacobson, S. J. Visco, L. C. De Jonghe, *Nano Letters* **2007**, *7*, 2136.
[50] C. H. Chen, M. H. J. Emond, E. M. Kelder, B. Meester, J. Schoonman, *Journal of Aerosol Science* **1999**, *30*, 959.

[51] D. Marinha, C. Rossignol, E. Djurado, *Journal of Solid State Chemistry* **2009**, *182*, 1742.
[52] O. Celikbilek, L. Dessemond, E. Djurado, *ECS Transactions* **2017**, *78*, 747.
[53] C. B. Carter, M. G. Norton, *Ceramic Materials [E-Book] : Science and Engineering*, 2nd ed. 2013. ed., Springer, New York, NY, **2013**.
[54] M. N. Rahaman, *CRC Press* **2003**, *2nd edition*.
[55] K. Kendall, in *High-Temperature Solid Oxide Fuel Cells for the 21st Century (Second Edition)*, Academic Press, Boston, **2016**, pp. 25.
[56] Y. Gong, C. Qin, K. Huang, *ECS Electrochemistry Letters* **2012**, *2*, F4.
[57] D. Klotz, A. Weber, E. Ivers-Tiffée, *Electrochimica Acta* **2017**, *227*, 110.
[58] E. Matte, G. Holzlechner, L. Epple, D. Stolten, P. Lupetin, *Journal of Power Sources* **2019**, *413*, 334.
[59] F. Wankmüller, M. Meffert, N. Russner, A. Weber, J. Schmieg, H. Störmer, T. Dickel, P. Lupetin, N. Maier, D. Gerthsen, E. Ivers-Tiffée, *J Mater Sci* **2020**, *55*, 11120.
[60] F. Grimm, N. H. Menzler, O. Guillon, *Journal of Power Sources* **2020**, *451*, 227607.
[61] M. Haydn, K. Ortner, T. Franco, S. Uhlenbruck, N. H. Menzler, D. Stöver, G. Bräuer, A. Venskutonis, L. S. Sigl, H.-P. Buchkremer, R. Vaßen, *Journal of Power Sources* **2014**, *256*, 52.
[62] J. Zhang, C. Lenser, N. H. Menzler, O. Guillon, *Solid State Ionics* **2020**, *344*, 115138.
[63] N. Jordan, W. Assenmacher, S. Uhlenbruck, V. A. C. Haanappel, H. P. Buchkremer, D. Stöver, W. Mader, *Solid State Ionics* **2008**, *179*, 919.
[64] R. Knibbe, J. Hjelm, M. Menon, N. Pryds, M. Søgaard, H. J. Wang, K. Neufeld, *Journal of the American Ceramic Society* **2010**, *93*, 2877.
[65] H. S. Noh, J. W. Son, H. Lee, J. S. Park, H. W. Lee, J. H. Lee, *Fuel Cells* **2010**, *10*, 1057.
[66] M. Sase, D. Ueno, K. Yashiro, A. Kaimai, T. Kawada, J. Mizusaki, *Journal of Physics and Chemistry of Solids* **2005**, *66*, 343.
[67] S. Uhlenbruck, N. Jordan, D. Sebold, H. P. Buchkremer, V. A. C. Haanappel, D. Stöver, *Thin Solid Films* **2007**, *515*, 4053.
[68] S. Uhlenbruck, T. Moskalewicz, N. Jordan, H. J. Penkalla, H. P. Buchkremer, *Solid State Ionics* **2009**, *180*, 418.
[69] J. Szász, F. Wankmüller, V. Wilde, H. Störmer, D. Gerthsen, N. H. Menzler, E. Ivers-Tiffée, *Journal of The Electrochemical Society* **2018**, *165*, F898.
[70] T. Ishihara, H. Matsuda, Y. Takita, *Journal of the American Chemical Society* **1994**, *116*, 3801.
[71] K. Huang, R. S. Tichy, J. B. Goodenough, *Journal of the American Ceramic Society* **1998**, *81*, 2565.
[72] K. Huang, R. S. Tichy, J. B. Goodenough, *Journal of the American Ceramic Society* **1998**, *81*, 2576.
[73] K. Huang, R. Tichy, J. B. Goodenough, C. Milliken, *Journal of the American Ceramic Society* **1998**, *81*, 2581.
[74] L. Blum, L. G. J. de Haart, J. Malzbender, N. H. Menzler, J. Remmel, R. Steinberger-Wilckens, *Journal of Power Sources* **2013**, *241*, 477.
[75] F. Han, R. Mücke, T. Van Gestel, A. Leonide, N. H. Menzler, H. P. Buchkremer, D. Stöver, *Journal of Power Sources* **2012**, *218*, 157.

[76] Q. Fang, L. Blum, N. H. Menzler, *Journal of The Electrochemical Society* **2015**, *162*, F907.
[77] C. Lenser, J. Zurek, D. Naumenko, C.-A. Thieu, J.-W. Son, U. de Haart, Q. Fang, L. Blum, N. H. Menzler, *Journal of Power Sources* **2020**, *474*, 228671.
[78] S. P. Jiang, S. H. Chan, *J Mater Sci* **2004**, *39*, 4405.
[79] W. C. Chueh, Y. Hao, W. Jung, S. M. Haile, *Nature Materials* **2011**, *11*, 155.
[80] M. Gerstl, A. Hutterer, J. Fleig, M. Bram, A. K. Opitz, *Solid State Ionics* **2016**, *298*, 1.
[81] M. Gerstl, A. Nenning, R. Iskandar, V. Rojek-Wöckner, M. Bram, H. Hutter, A. Opitz, *Materials* **2016**, *9*, 649.
[82] T. Nakamura, K. Yashiro, A. Kaimai, T. Otake, K. Sato, T. Kawada, J. Mizusaki, *Journal of The Electrochemical Society* **2008**, *155*, B1244.
[83] V. A. Rojek-Wöckner, A. K. Opitz, M. Brandner, J. Mathé, M. Bram, *Journal of Power Sources* **2016**, *328*, 65.
[84] C. Lenser, N. H. Menzler, *Solid State Ionics* **2019**, *334*, 70.
[85] D. Burnat, G. Nurk, L. Holzer, M. Kopecki, A. Heel, *Journal of Power Sources* **2018**, *385*, 62.
[86] Y. Huan, Y. Li, B. Yin, D. Ding, T. Wei, *Journal of Power Sources* **2017**, *359*, 384.
[87] Y.-H. Huang, R. I. Dass, Z.-L. Xing, J. B. Goodenough, *Science* **2006**, *312*, 254.
[88] X. Kong, X. Zhou, Y. Tian, X. Wu, J. Zhang, W. Zuo, X. Gong, Z. Guo, *Journal of Power Sources* **2016**, *316*, 224.
[89] Y.-F. Sun, Y.-Q. Zhang, B. Hua, Y. Behnamian, J. Li, S.-H. Cui, J.-H. Li, J.-L. Luo, *Journal of Power Sources* **2016**, *301*, 237.
[90] Z. Xu, Y.-M. Yin, J. Lu, L. Xu, N. Zhou, J.-W. Yin, Z.-F. Ma, *Journal of The Electrochemical Society* **2016**, *163*, F737.
[91] X. Shen, K. Sasaki, *Journal of Power Sources* **2016**, *320*, 180.
[92] L. De Rogatis, M. Cargnello, V. Gombac, B. Lorenzut, T. Montini, P. Fornasiero, *ChemSusChem* **2010**, *3*, 24.
[93] O. Kwon, S. Sengodan, K. Kim, G. Kim, H. Y. Jeong, J. Shin, Y.-W. Ju, J. W. Han, G. Kim, *Nature Communications* **2017**, *8*, 15967.
[94] D. Neagu, G. Tsekouras, D. N. Miller, H. Ménard, J. T. S. Irvine, *Nature Chemistry* **2013**, *5*, 916.
[95] A. M. Dayaghi, K. J. Kim, S. Kim, J. Park, S. J. Kim, B. H. Park, G. M. Choi, *Journal of Power Sources* **2016**, *324*, 288.
[96] Y. Gao, D. Chen, M. Saccoccio, Z. Lu, F. Ciucci, *Nano Energy* **2016**, *27*, 499.
[97] A. Nenning, L. Volgger, E. Miller, L. V. Mogni, S. Barnett, J. Fleig, *Journal of The Electrochemical Society* **2017**, *164*, F364.
[98] X. Shen, T. Chen, S. R. Bishop, N. H. Perry, H. L. Tuller, K. Sasaki, *Journal of Power Sources* **2017**, *370*, 122.
[99] N. Zhou, Y.-M. Yin, Z. Chen, Y. Song, J. Yin, D. Zhou, Z.-F. Ma, *Journal of The Electrochemical Society* **2018**, *165*, F629.
[100] J. T. S. Irvine, D. Neagu, M. C. Verbraeken, C. Chatzichristodoulou, C. Graves, M. B. Mogensen, *Nature Energy* **2016**, *1*, 15014.
[101] S. B. Adler, J. A. Lane, B. C. H. Steele, *Journal of The Electrochemical Society* **1996**, *143*, 3554.
[102] T. Ishihara, *Perovskite oxide for solid oxide fuel cells*, Springer, Dordrecht, **2009**.

[103] N. Q. Minh, T. Takahashi, in *Science and Technology of Ceramic Fuel Cells*, Elsevier Science Ltd, Oxford, **1995**, pp. 117.
[104] S. J. Kim, A. M. Dayaghi, K. J. Kim, G. M. Choi, *Journal of Power Sources* **2017**, *344*, 218.
[105] H. Shimada, T. Yamaguchi, H. Sumi, K. Nomura, Y. Yamaguchi, Y. Fujishiro, *Journal of Power Sources* **2017**, *341*, 280.
[106] A. Mai, V. A. C. Haanappel, S. Uhlenbruck, F. Tietz, D. Stöver, *Solid State Ionics* **2005**, *176*, 1341.
[107] J. Nielsen, Å. H. Persson, T. T. Muhl, K. Brodersen, *Journal of The Electrochemical Society* **2018**, *165*, F90.
[108] J. H. Park, S. M. Han, K. J. Yoon, H. Kim, J. Hong, B.-K. Kim, J.-H. Lee, J.-W. Son, *Journal of Power Sources* **2016**, *315*, 324.
[109] D. Udomsilp, J. Rechberger, R. Neubauer, C. Bischof, F. Thaler, W. Schafbauer, N. H. Menzler, L. G. J. de Haart, A. Nenning, A. K. Opitz, O. Guillon, M. Bram, *Cell Reports Physical Science* **2020**, *1*.
[110] Z. Shao, S. M. Haile, *Nature* **2004**, *431*, 170.
[111] H. Ullmann, N. Trofimenko, F. Tietz, D. Stöver, A. Ahmad-Khanlou, *Solid State Ionics* **2000**, *138*, 79.
[112] B. Wei, Z. Lü, X. Huang, J. Miao, X. Sha, X. Xin, W. Su, *Journal of the European Ceramic Society* **2006**, *26*, 2827.
[113] S. Baumann, W. A. Meulenberg, H. P. Buchkremer, *Journal of the European Ceramic Society* **2013**, *33*, 1251.
[114] A. Beez, X. Yin, N. H. Menzler, R. Spatschek, M. Bram, *Journal of The Electrochemical Society* **2017**, *164*, F3028.
[115] L. Gao, Q. Li, L. Sun, X. Zhang, L. Huo, H. Zhao, J.-C. Grenier, *Journal of Power Sources* **2017**, *371*, 86.
[116] N. V. Lyskov, L. M. Kolchina, M. Z. Galin, G. N. Mazo, *Solid State Ionics* **2018**, *319*, 156.
[117] S. Pang, W. Wang, T. Chen, X. Shen, Y. Wang, K. Xu, X. Xi, *Journal of Power Sources* **2016**, *326*, 176.
[118] C. Berger, E. Bucher, C. Gspan, W. Sitte, *Journal of Solid State Chemistry* **2019**, *273*, 92.
[119] C. Berger, E. Bucher, A. Windischbacher, A. D. Boese, W. Sitte, *Journal of Solid State Chemistry* **2018**, *259*, 57.
[120] Y. Yamaguchi, I. Kagomiya, S. Minami, H. Shimada, H. Sumi, Y. Ogura, Y. Mizutani, *Journal of Power Sources* **2020**, *448*, 227426.
[121] R. K. Sharma, M. Burriel, L. Dessemond, J.-M. Bassat, E. Djurado, *Journal of Power Sources* **2016**, *325*, 337.
[122] R. K. Sharma, M. Burriel, L. Dessemond, V. Martin, J.-M. Bassat, E. Djurado, *Journal of Power Sources* **2016**, *316*, 17.
[123] R. K. Sharma, S.-K. Cheah, M. Burriel, L. Dessemond, J.-M. Bassat, E. Djurado, *Journal of Materials Chemistry A* **2017**, *5*, 1120.
[124] V. Vibhu, A. Rougier, C. Nicollet, A. Flura, S. Fourcade, N. Penin, J.-C. Grenier, J.-M. Bassat, *Journal of Power Sources* **2016**, *317*, 184.
[125] S. Joo, J. Kim, J. Shin, T.-H. Lim, G. Kim, *Journal of The Electrochemical Society* **2016**, *163*, F1489.

[126] J. Sun, X. Liu, F. Han, L. Zhu, H. Bi, H. Wang, S. Yu, L. Pei, *Solid State Ionics* **2016**, *288*, 54.
[127] V. Dusastre, J. A. Kilner, *Solid State Ionics* **1999**, *126*, 163.
[128] H. J. Hwang, J.-W. Moon, S. Lee, E. A. Lee, *Journal of Power Sources* **2005**, *145*, 243.
[129] J. Nielsen, T. Jacobsen, M. Wandel, *Electrochimica Acta* **2011**, *56*, 7963.
[130] E. Perry Murray, M. J. Sever, S. A. Barnett, *Solid State Ionics* **2002**, *148*, 27.
[131] R. Wang, F. Jin, L. Ta, T. He, *Solid State Ionics* **2016**, *288*, 32.
[132] W. Zhang, J. Meng, X. Zhang, L. Zhang, X. Liu, J. Meng, *Solid State Ionics* **2018**, *316*, 20.
[133] A. S. Painter, Y.-L. Huang, E. D. Wachsman, *Journal of Power Sources* **2017**, *360*, 391.
[134] J. Hou, L. Bi, J. Qian, Z. Gong, Z. Zhu, W. Liu, *Journal of Power Sources* **2016**, *301*, 306.
[135] Z. Zhang, Y. Zhu, Y. Zhong, W. Zhou, Z. Shao, *Advanced Energy Materials* **2017**, *7*, 1700242.
[136] W. Sun, P. Li, C. Xu, L. Dong, J. Qiao, Z. Wang, D. Rooney, K. Sun, *Journal of Power Sources* **2017**, *343*, 237.
[137] J. Nielsen, Å. H. Persson, B. R. Sudireddy, J. T. S. Irvine, K. Thydén, *Journal of Power Sources* **2017**, *372*, 99.
[138] Q. Ma, S. Dierickx, V. Vibhu, D. Sebold, L. G. J. de Haart, A. Weber, O. Guillon, N. H. Menzler, *Journal of The Electrochemical Society* **2020**, *167*, 084522.
[139] S. Pang, W. Wang, Y. Su, X. Shen, Y. Wang, K. Xu, C. Chen, *Journal of The Electrochemical Society* **2017**, *164*, F775.
[140] X. Meng, Y. Shen, M. Xie, Y. Yin, N. Yang, Z.-F. Ma, J. C. Diniz da Costa, S. Liu, *Journal of Power Sources* **2016**, *306*, 226.
[141] F. Dong, M. Ni, W. He, Y. Chen, G. Yang, D. Chen, Z. Shao, *Journal of Power Sources* **2016**, *326*, 459.
[142] L. Zhang, S. Li, T. Xia, L. Sun, L. Huo, H. Zhao, *International Journal of Hydrogen Energy* **2018**, *43*, 3761.
[143] A. Chrzan, S. Ovtar, P. Jasinski, M. Chen, A. Hauch, *Journal of Power Sources* **2017**, *353*, 67.
[144] Y.-f. Bu, Q. Zhong, D.-C. Chen, Y. Chen, S. Y. Lai, T. Wei, H.-b. Sun, D. Ding, M. Liu, *Journal of Power Sources* **2016**, *319*, 178.
[145] D. Y. Jang, M. Kim, J. W. Kim, K. Bae, J.-w. Son, M. V. F. Schlupp, J. H. Shim, *Journal of The Electrochemical Society* **2017**, *164*, F484.
[146] H. Shimada, T. Yamaguchi, T. Suzuki, H. Sumi, K. Hamamoto, Y. Fujishiro, *Journal of Power Sources* **2016**, *302*, 308.
[147] G. M. Rupp, A. Schmid, A. Nenning, J. Fleig, *Journal of The Electrochemical Society* **2016**, *163*, F564.
[148] H. Qi, Z. Zhao, B. Tu, M. Cheng, *Journal of Power Sources* **2020**, *455*, 227971.
[149] S. Ovtar, M. Chen, A. J. Samson, R. Kiebach, *Solid State Ionics* **2017**, *304*, 51.
[150] H.-S. Noh, K. J. Yoon, B.-K. Kim, H.-J. Je, H.-W. Lee, J.-H. Lee, J.-W. Son, *Journal of Power Sources* **2014**, *247*, 105.
[151] R. T. Leah, A. Bone, E. Hammer, A. Selcuk, M. Rahman, A. Clare, L. Rees, N. Lawrence, A. Ballard, T. Domanski, S. Mukerjee, M. Selby, *ECS Transactions* **2017**, *78*, 2005.

[152] M. Haydn, C. Bischof, D. Udomsilp, A. K. Opitz, G. Bimashofer, W. Schafbauer, M. Brandner, M. Bram, *ECS Transactions* **2017**, *78*, 1993.
[153] E. Dogdibegovic, R. Wang, G. Y. Lau, M. C. Tucker, *Journal of Power Sources* **2019**, *410-411*, 91.
[154] S. Zhen, W. Sun, P. Li, G. Tang, D. Rooney, K. Sun, X. Ma, *Journal of Power Sources* **2016**, *315*, 140.
[155] L. Shao, P. Wang, Q. Zhang, L. Fan, N. Zhang, K. Sun, *Journal of Power Sources* **2017**, *343*, 268.
[156] L. Ding, L. Wang, D. Ding, S. Zhang, X. Ding, G. Yuan, *Journal of Power Sources* **2017**, *354*, 26.
[157] K.-J. Pan, A. M. Hussain, E. D. Wachsman, *Journal of Power Sources* **2017**, *347*, 277.
[158] L. dos Santos-Gómez, J. M. Porras-Vázquez, E. R. Losilla, F. Martín, J. R. Ramos-Barrado, D. Marrero-López, *Journal of Power Sources* **2017**, *347*, 178.
[159] T. Hong, K. Brinkman, C. Xia, *Journal of Power Sources* **2016**, *329*, 281.
[160] Ö. Çelikbilek, D. Jauffrès, E. Siebert, L. Dessemond, M. Burriel, C. L. Martin, E. Djurado, *Journal of Power Sources* **2016**, *333*, 72.
[161] E. Commission, *European Green Deal*, **2019**, access: 02 March 2020, https://ec.europa.eu/info/strategy/priorities-2019-2024/european-green-deal_en
[162] E. Commission, *2030 climate & energy framework*, **2019**, access: 02 March 2020, https://ec.europa.eu/clima/policies/strategies/2030_en
[163] S. Foit, L. Dittrich, T. Duyster, I. Vinke, R.-A. Eichel, L. G. J. de Haart, *Processes* **2020**, *8*, 1390.
[164] M. S. Khan, X. Xu, J. Zhao, R. Knibbe, Z. Zhu, *Journal of Power Sources* **2017**, *359*, 104.
[165] A. Hauch, K. Brodersen, M. Chen, C. Graves, S. H. Jensen, P. S. Jørgensen, P. V. Hendriksen, M. B. Mogensen, S. Ovtar, X. Sun, *ECS Transactions* **2017**, *75*, 3.
[166] R. Knibbe, M. L. Traulsen, A. Hauch, S. D. Ebbesen, M. Mogensen, *Journal of The Electrochemical Society* **2010**, *157*, B1209.
[167] V. Vibhu, S. Yildiz, I. C. Vinke, R.-A. Eichel, J.-M. Bassat, L. G. J. de Haart, *Journal of The Electrochemical Society* **2019**, *166*, F102.
[168] M. Liu, M. G. Millan-Agorio, P. V. Aravind, N. P. Brandon, *Influence of Operation Conditions on Carbon Deposition in SOFCs Fuelled by Tar-Containing Biosyngas, Vol. 158*, **2011**.
[169] N. Bogolowski, B. Iwanschitz, J.-F. Drillet, *Fuel Cells* **2015**, *15*, 711.
[170] H. Jeong, *Coupling a solid oxide fuel cell with a biomass gasifier : degradation mechanisms and alternative anode materials, Vol. 460*, Forschungszentrum, Zentralbibliothek, Jülich, **2019**.
[171] M. Miyake, S. Matsumoto, M. Iwami, S. Nishimoto, Y. Kameshima, *International Journal of Hydrogen Energy* **2016**, *41*, 13625.
[172] M. Miyake, M. Iwami, M. Takeuchi, S. Nishimoto, Y. Kameshima, *Journal of Power Sources* **2018**, *390*, 181.
[173] M. B. Mogensen, A. Hauch, X. Sun, M. Chen, Y. Tao, S. D. Ebbesen, K. V. Hansen, P. V. Hendriksen, *Fuel Cells* **2017**, *17*, 434.
[174] M. P. Hoerlein, M. Riegraf, R. Costa, G. Schiller, K. A. Friedrich, *Electrochimica Acta* **2018**, *276*, 162.

[175] Q. Fang, C. E. Frey, N. H. Menzler, L. Blum, *Journal of The Electrochemical Society* **2018**, *165*, F38.
[176] C. E. Frey, Q. Fang, D. Sebold, L. Blum, N. H. Menzler, *Journal of The Electrochemical Society* **2018**, *165*, F357.
[177] A. Hauch, K. Brodersen, M. Chen, M. B. Mogensen, *Solid State Ionics* **2016**, *293*, 27.
[178] G. Rinaldi, A. Nakajo, P. Caliandro, L. Navratilova, J. Van herle, *ECS Transactions* **2019**, *91*, 641.
[179] Z. Jiao, N. Shikazono, *Journal of Power Sources* **2018**, *396*, 119.
[180] M. Trini, A. Hauch, S. De Angelis, X. Tong, P. V. Hendriksen, M. Chen, *Journal of Power Sources* **2020**, *450*, 227599.
[181] N. H. Menzler, D. Sebold, Y. J. Sohn, S. Zischke, *Journal of Power Sources* **2020**, *478*, 228770.
[182] T. Ishihara, S. Wang, K.-T. Wu, *Solid State Ionics* **2017**, *299*, 60.
[183] C. Zhu, L. Hou, S. Li, L. Gan, K. Xie, *Journal of Power Sources* **2017**, *363*, 177.
[184] J. Yan, Z. Zhao, L. Shang, D. Ou, M. Cheng, *Journal of Power Sources* **2016**, *319*, 124.
[185] H. Zheng, Y. Tian, L. Zhang, B. Chi, J. Pu, L. Jian, *Journal of Power Sources* **2018**, *383*, 93.
[186] X. Tong, S. Ovtar, K. Brodersen, P. V. Hendriksen, M. Chen, *Journal of Power Sources* **2020**, *451*, 227742.
[187] E. Dogdibegovic, F. Shen, R. Wang, I. Robinson, G. Y. Lau, M. C. Tucker, *ECS Transactions* **2019**, *91*, 877.
[188] K. D. Kreuer, *Annual Review of Materials Research* **2003**, *33*, 333.
[189] E. Fabbri, D. Pergolesi, E. Traversa, *Chemical Society Reviews* **2010**, *39*, 4355.
[190] G. Taillades, P. Pers, V. Mao, M. Taillades, *International Journal of Hydrogen Energy* **2016**, *41*, 12330.
[191] L. Yang, S. Wang, K. Blinn, M. Liu, Z. Liu, Z. Cheng, M. Liu, *Science* **2009**, *326*, 126.
[192] C. Duan, J. Tong, M. Shang, S. Nikodemski, M. Sanders, S. Ricote, A. Almansoori, R. O'Hayre, *Science* **2015**, *349*, 1321.
[193] H. An, H.-W. Lee, B.-K. Kim, J.-W. Son, K. J. Yoon, H. Kim, D. Shin, H.-I. Ji, J.-H. Lee, *Nature Energy* **2018**, *3*, 870.
[194] N. H. Menzler, W. Schafbauer, R. Mücke, R. Kauert, O. Büchler, H. P. Buchkremer, D. Stöver, in *Ceramic Engineering and Science Proceedings, Vol. 32*, 4 ed., **2011**, pp. 149.
[195] R. Mücke, N. H. Menzler, H. P. Buchkremer, D. Stöver, *Journal of the American Ceramic Society. Jan2009 Supplement, Vol. 92, pS95-S102. 8p. 4 Black and White Photographs, 2 Charts, 8 Graphs.* **2009**, *92*, Start Page: S95.
[196] E. Forster, D. van Holt, M. E. Ivanova, S. Baumann, W. A. Meulenberg, M. Müller, *Journal of the European Ceramic Society* **2016**, *36*, 3457.
[197] R. Haugsrud, *Solid State Ionics* **2007**, *178*, 555.
[198] D. van Holt, E. Forster, M. E. Ivanova, W. A. Meulenberg, M. Müller, S. Baumann, R. Vaßen, *Journal of the European Ceramic Society* **2014**, *34*, 2381.
[199] K. Leonard, Y. Okuyama, Y. Takamura, Y.-S. Lee, K. Miyazaki, M. E. Ivanova, W. A. Meulenberg, H. Matsumoto, *Journal of Materials Chemistry A* **2018**, *6*, 19113.

[200] M. Marrony, *Proton-conducting ceramics : from fundamentals to applied research*, Pan Stanford, Singapore, **2016**.
[201] H. Ding, N. P. Sullivan, S. Ricote, *Solid State Ionics* **2017**, *306*, 97.
[202] E. Fabbri, S. Licoccia, E. Traversa, E. D. Wachsman, *Fuel Cells* **2009**, *9*, 128.
[203] M. E. Ivanova, S. Escolástico, M. Balaguer, J. Palisaitis, Y. J. Sohn, W. A. Meulenberg, O. Guillon, J. Mayer, J. M. Serra, *Scientific Reports* **2016**, *6*, 34773.
[204] L. Yang, Z. Liu, S. Wang, Y. Choi, C. Zuo, M. Liu, *Journal of Power Sources* **2010**, *195*, 471.
[205] D. Han, Y. Okumura, Y. Nose, T. Uda, *Solid State Ionics* **2010**, *181*, 1601.
[206] S. Choi, C. J. Kucharczyk, Y. Liang, X. Zhang, I. Takeuchi, H.-I. Ji, S. M. Haile, *Nature Energy* **2018**, *3*, 202.
[207] L. Fan, P.-C. Su, *Journal of Power Sources* **2016**, *306*, 369.
[208] H. Téllez Lozano, J. Druce, S. J. Cooper, J. A. Kilner, *Science and Technology of Advanced Materials* **2017**, *18*, 977.
[209] J. Dailly, M. Marrony, G. Taillades, M. Taillades-Jacquin, A. Grimaud, F. Mauvy, E. Louradour, J. Salmi, *Journal of Power Sources* **2014**, *255*, 302.
[210] R. Strandbakke, V. A. Cherepanov, A. Y. Zuev, D. S. Tsvetkov, C. Argirusis, G. Sourkouni, S. Prünte, T. Norby, *Solid State Ionics* **2015**, *278*, 120.
[211] R. Strandbakke, E. Vøllestad, S. A. Robinson, M.-L. Fontaine, T. Norby, *Journal of The Electrochemical Society* **2017**, *164*, F196.
[212] G. Li, H. Jin, Y. Cui, L. Gui, B. He, L. Zhao, *Journal of Power Sources* **2017**, *341*, 192.
[213] S. Wang, J. Shen, Z. Zhu, Z. Wang, Y. Cao, X. Guan, Y. Wang, Z. Wei, M. Chen, *Journal of Power Sources* **2018**, *387*, 24.
[214] L. Zhao, G. Li, K. Chen, Y. Ling, Y. Cui, L. Gui, B. He, *Journal of Power Sources* **2016**, *333*, 24.
[215] C. Duan, R. Kee, H. Zhu, N. Sullivan, L. Zhu, L. Bian, D. Jennings, R. O'Hayre, *Nature Energy* **2019**, *4*, 230.
[216] S. Choi, T. C. Davenport, S. M. Haile, *Energy & Environmental Science* **2019**, *12*, 206.
[217] L. Gui, Y. Ling, G. Li, Z. Wang, Y. Wan, R. Wang, B. He, L. Zhao, *Journal of Power Sources* **2016**, *301*, 369.
[218] Z. Chen, J. Wang, D. Huan, S. Sun, G. Wang, Z. Fu, W. Zhang, X. Zheng, H. Pan, R. Peng, Y. Lu, *Journal of Power Sources* **2017**, *371*, 41.
[219] A. R. Hanifi, N. K. Sandhu, T. H. Etsell, J.-L. Luo, P. Sarkar, *Journal of Power Sources* **2017**, *341*, 264.
[220] Y. Wan, B. He, R. Wang, Y. Ling, L. Zhao, *Journal of Power Sources* **2017**, *347*, 14.
[221] J. Kim, A. Jun, O. Gwon, S. Yoo, M. Liu, J. Shin, T.-H. Lim, G. Kim, *Nano Energy* **2018**, *44*, 121.
[222] W. Wu, H. Ding, Y. Zhang, Y. Ding, P. Katiyar, P. K. Majumdar, T. He, D. Ding, *Advanced Science* **2018**, *5*, 1800360.